University of Alberta

Effects of Oxide Additions on the Corrosion Behaviour of Cr_2O_3 Based Ceramics in High Temperature Supercritical Water Environment

by

Renfei Wang

A thesis submitted to the Faculty of Graduate Studies and Research
in partial fulfillment of the requirements for the degree of

Master of Science

Chemical and Materials Engineering

Fall 2012
Edmonton, Alberta

Abstract

This investigation is aimed at developing ceramic materials applied in supercritical water, which is being considered as coolant for one of the next generation nuclear reactors. Cr_2O_3, a primary protective film on stainless steels, was found to be unstable in SCW due to the formation of soluble Cr^{6+} species, which can be severed by increasing the oxygen content in SCW or by reducing the ceramic's grain size. To enhance the stability of Cr_2O_3 in SCW, various amounts of other oxides including MgO, CeO_2 and SiO_2 additives were added into Cr_2O_3 and these ceramics were exposed to an SCW environment at 650 ℃/25 MPa for up to 600 hours. The results showed that adding a proper amount (less than 5 wt. %) of CeO_2 and MgO into Cr_2O_3 can increase the corrosion resistance of Cr_2O_3 based ceramics in SCW environments, whereas high additions content can deteriorate the stability of Cr_2O_3 based ceramics.

Acknowledgements

To begin with, I would like to express my genuine gratitude to my supervisors, Dr. Jingli Luo and Dr. Weixing Chen, whose constant guidance and encouragement have been a valuable resource of inspiration during my two years' master study. Their diligence and conscientiousness also set up a role model that will continue benefiting me in my future work and study.

The funding provided by Natural Resource of Canada (NRCan), Atomic Energy of Canada Limited (AECL) and Natural Science and Engineering Research Council of Canada (NCERC) is sincerely appreciated.

Special thanks are given to Mr. Ziqiang Dong, who selflessly offered countless assistance and constructive opinions for experiment setup, data analysis as well as technical writing. I would also like take this opportunity to thank other members in our group, Dr. Ming Li, Mr. Yashar Behnanmian and Mr. Zhe Liu, for lending me precious help and teaching me the true meaning of "teamwork".

Last but not the least, I am deeply indebted to my beloved parents, Lihong Ren and Baoquan Wang, who taught me to be self-motivated and to bravely face whatever challenge that might be in store for me.

Table of Contents

List of Tables

List of Figures

Chapter 1 Introduction

1.1 Supercritical water cooled reactors

Nuclear power is increasingly playing a crucial role in 21st century due to its clean and carbon-free nature. Nevertheless, generation II and III reactors which were currently in operation, such as light water reactor (LWR) and pressurized water reactor (PWR), bring concerns regarding to their safety, efficiency and operating cost. Generation IV International Forum (GIF) has been focused on developing new generation nuclear reactors to overcome the aforementioned deficiencies. As one of the six nuclear power reactors proposed by GIF, supercritical water cooled reactor (SCWR) has attracted tremendous attentions. SCWR uses water near or above its critical point (374℃, 22.1 MPa) as coolant, and its operating temperature and pressure are shown in Figure 1-1.

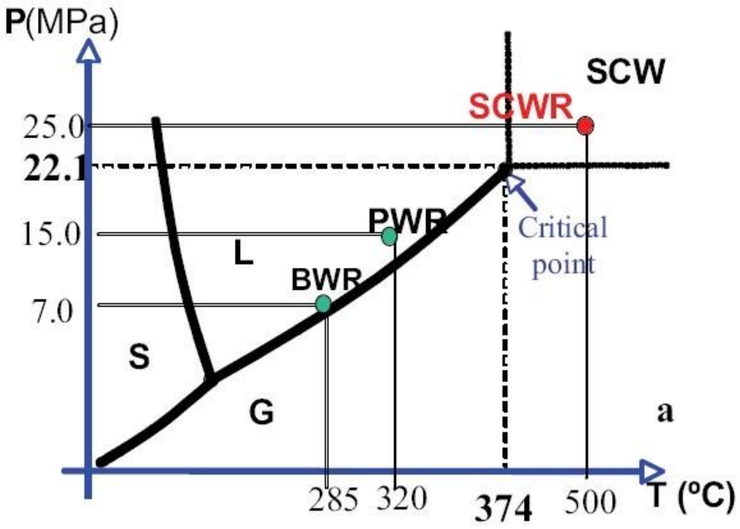

Figure 1-1. Pressure and temperature regimes of SCWR, PWR and BWR [1].

It has been found that supercritical water possesses unique properties comparing to the ambient liquid water. As the temperature and pressure proceed to the critical point, the density of the water will diminish rapidly to the extent that no distinguishable boundary between liquidus and gaseous phase can be observed. Hydrogen bonding becomes weaker at supercritical state, resulting in the complete miscibility of organics, and insolubility of inorganic species [2]. It was found that across the pseudo-critical zone, water showed enhanced heat transfer, as can be seen from Figure 1-2. Therefore, when using supercritical water as coolant for the nuclear reactor, efficiency will be increased dramatically (over 45% comparing to 30% for the current generation of reactors). Moreover, since there is no phase change involved in SCWR, components such as steam generators or separators can be eliminated, which leads to greater configuration simplicity of the reactor [3].

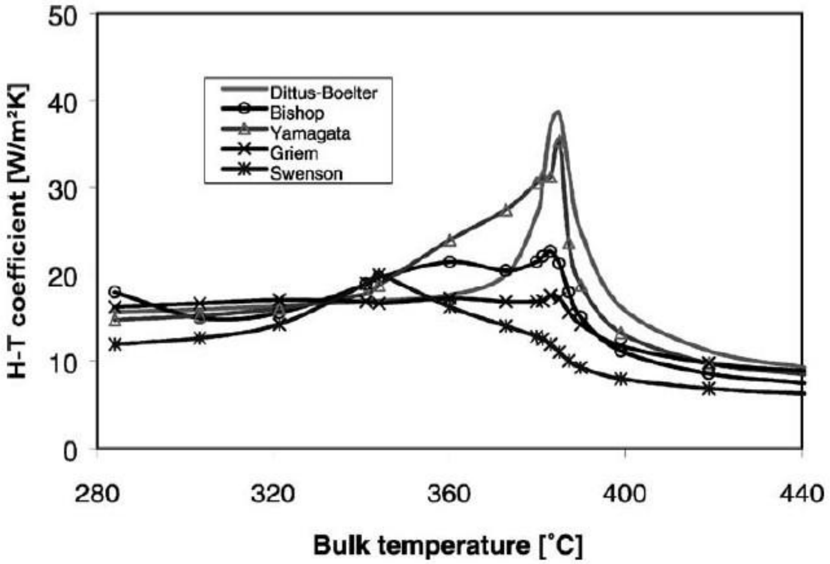

Figure 1-2. Different heat transfer correlations at supercritical pressures [4].

SCWR can be designed either as a thermal reactor with once-through fuel cycle, or as a fast reactor with closed fuel cycle [5]. As the study of SCWR carried on world widely, mainly two concepts of the SCWR designs have been proposed [3, 6~8]. In Canada, the CANDU®-SCWR concept has been developed as a thermal reactor, and its general structure is shown in Figure 1-3. In CANDU®-SCWR design, the use of multi-pass reactor flows further enhances thermal efficiency, and its flexibility and safety can also be improved [9]. The preliminary operating parameters of the CANDU®-SCWR are presented in Table 1-1.

Table 1-1. Preliminary parameters of CANDU®-SCWR [10, 11].

Reactor spectrum	Thermal
Moderator	Heavy water
Coolant	Light water
Thermal Power	2540 MW
Electrical Power	1220 MW
Thermal efficiency	48%
Flow rate	1320 kg/s
Fuel	UO2/Th
Enrichment	4 wt.%
Number of channels	300
Core diameter	4 m
Pressure	25 MPa
Inlet temperature	350 ℃
Outlet temperature	625 ℃
Cladding temperature	< 850 ℃

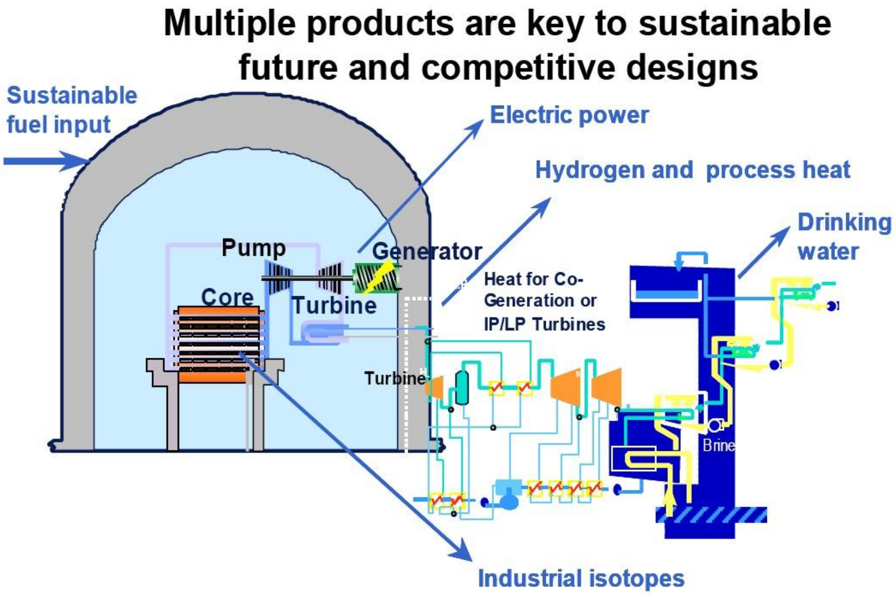

Figure 1-3. Schematic of general structure of CANDU®-SCWR [10].

1.2 Candidate materials for SCWR

1.2.1 Fuel channel design and materials requirements

In CANDU®-SCW, the continuing utilization of low neutron absorbing materials requires new design of the fuel channel, and currently two concepts of design are under consideration [11]. Figure 1-4 illustrates the High Efficiency Channel (HEC) design. As can be seen from the figure, the pressure tube, which is in direct contact with the moderator, is thermally insulated from the hot coolant by an insulator. The HEC design offers higher level of simplicity due to the elimination of the calandria tubes which are used in the other design to separate the pressure tube from the moderator. Furthermore, the HEC design also enables SCWR to operate at much lower temperatures [10].

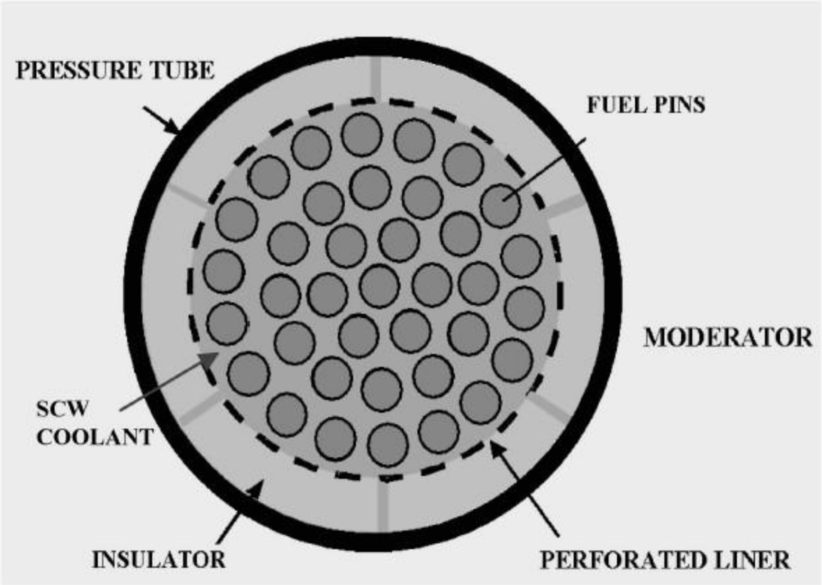

Figure 1-4. Schematic of the HEC CANDU®-SCWR fuel channel design [11].

The other concept, namely the Re-Entrant Channel (REC) design, is shown in Figure 1-5. In REC, a gas annulus is used to separate the pressure tube from the moderator. The coolant flows between the pressure tube and the inner tube, and then turns around to flow between the inner tubes. This design ensures the temperature of the pressure tube close to that of the inner tube, which is in the region of 300 ℃~400 ℃. The REC design avoids the potential problems existed in the HEC design, such as hydriding and blistering, caused by the inserted insulator which can be difficult to replace if corroded or cracked [12].

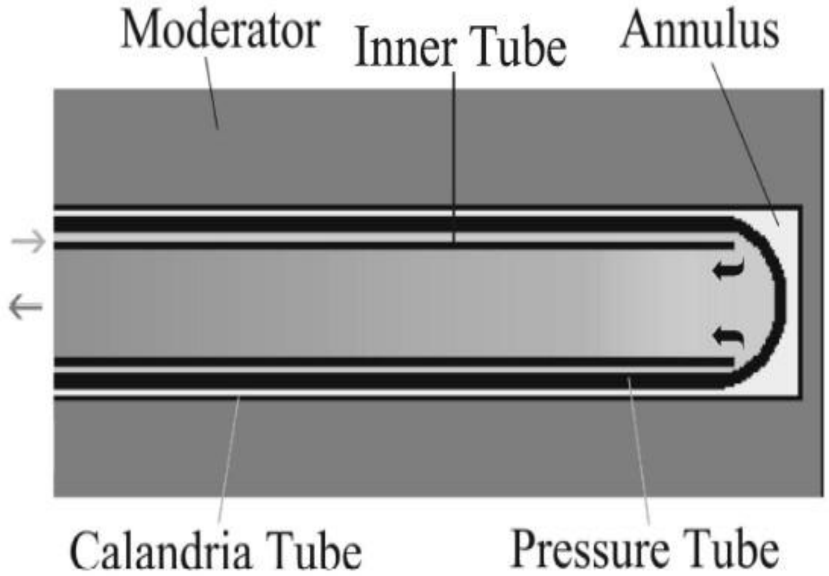

Figure 1-5. Schematic of the REC CANDU®-SCWR fuel channel design [11].

In both HEC and REC design, the pressure tubes operate at relatively low temperatures (about 80 ℃ for HEC and 350 ℃ for REC). Therefore, corrosion resistance may not be a major concern for the candidate materials. However, sufficient mechanical properties should be ensured to avoid creep, cracking or deformation at high pressures. The general requirements for the insulator are high thermal and corrosion resistance. It should also provide proper mechanical strength to support the load of the bundle, even though the pressure is not as high as that of the coolant. The creep property of the candidate insulator materials is also of great importance. The materials requirements of the liner tube in HEC and the inner tube in REC are excellent high temperature corrosion resistance, low swelling rate but not necessarily high mechanical strength. The high temperature irradiation stability of the materials should also be taken into consideration.

The main challenging part in the study of candidate materials in the CANDU®-SCWR is to develop materials that can withstand corrosion at temperature as high as 850 ℃. Coatings can be applied to enhance the corrosion resistance of the materials if necessary [11, 13].

1.2.2 Ferritic-martensitic steels

Ferritic-martensitic (F-M) steels show their superiority on their excellent mechanical properties, great irradiation resistance, low swelling and high thermal conductivity. Also, by controlling the alloying elements additions, their creep and corrosion resistance at elevated temperature can also be acceptable. Therefore, F-M steels have been considered as materials of choice for many proposed Gen IV reactor concepts. A detailed review on the studies of F-M alloys for the next generation reactors was given by Klueh et al [14].

Hwang et al. [15] examined the corrosion and stress cracking corrosion susceptibilities of two F-M steels, T91a and T92, in SCW at 500 ℃, 550 ℃ and 600 ℃. Great weight gain was observed after SCW test, especially for alloys exposed at 600 ℃. A series of F-M alloys including T91, HCM12A and HT-9 were tested in SCW environment by Ampornrat et al. [16] with temperatures varied from 400 ℃ to 600 ℃ and oxygen partial pressures from 10 ppb to 300 ppb. Among the samples examined, HT-9 exhibited the best corrosion resistance, followed by HCM12A and T91. The corrosion behaviors of P92 were studied at 500 ℃~600 ℃ and 25 MPa [17]. At 600 ℃, the steel showed severe oxidation and even developed cracks at the oxide scale. Chen et al. [18] investigated the supercritical water behaviors of T91 in two different dissolved oxygen levels (25 ppb and 2 ppm) at 500 ℃ for up to 505 hours. Tests at same conditions on HT-9 alloy were conducted by Ren et al. [19]. The effects of temperature (from 360 ℃~600 ℃) and exposure time (1~3000 hours) on the corrosion responses of NF616 and HCM12A in SCW environment were also examined [20].

It was found that the corrosion behaviors of F-M steels in SCW can be strongly affected by temperature, and when it exceeds 500 ℃ the weight gain of the steels follows parabolic law [16~21]. Figure 1-6 shows typical corrosion behaviors of several F-M steels in SCW at various temperatures.

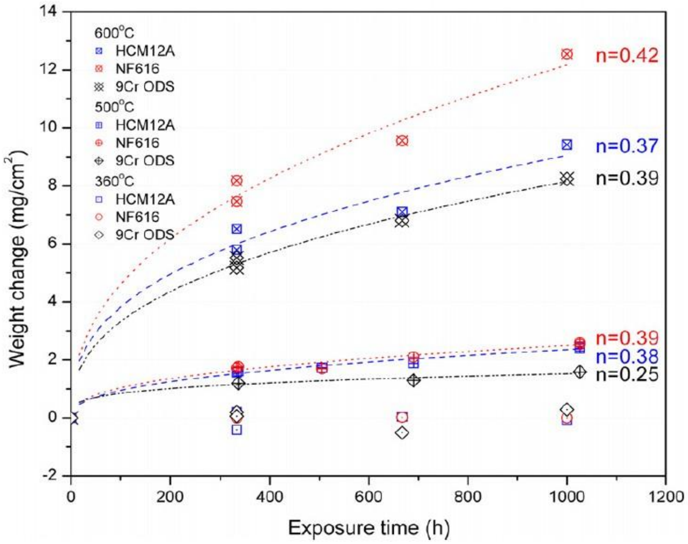

Figure 1-6. Weight changes of HCM12A, NF616 and 9Cr ODS exposed in supercritical and subcritical water environments at 600 ℃, 500 ℃ and 360 ℃, as a function of time [21].

Dissolved oxygen content is another key parameter that can exert substantial influence on the SCW corrosion of F-M steels. Studies showed that the oxide structure formed on the steels surface depended on the dissolved oxygen content of the SCW environment to which they were exposed. For F-M steels exposed to SCW at dissolved oxygen content, a dual-layer oxide can be commonly observed on the surface [16~21]. The outer layer was found to comprise significant amounts of Fe but be depleted with Cr, whereas the inner layer was enriched in both Fe and Cr. In addition, an internal oxide zone can be found beneath the inner layer, where the composition of the steel gradually changed, providing a transition between the substrate and the oxide layers. The chemical properties of those two layers have been analyzed by XRD and EBSD, and it was found that iron magnetite Fe_3O_4 constituted the outer layer whereas the inner layer contained iron spinel phase $(Fe, Cr)_3O_4$. The oxidation mechanism of F-M alloys has been explained by Ampornrat et al. [16] and Yin et al. [17]. The formation of outer layer, which was relatively porous and coarse, resulted from the outward diffusion of cations. Since Fe possesses a higher diffusion coefficient than Cr and Ni, it can diffuse through the spinel and magnetite layers and react with oxygen at the alloy surface, which accounted for the growth of the oxide scales. Oxygen diffusing into the steel reacted with Cr and Fe, resulting in the formation of spinel phases in the inner oxide layer. It was found that the short circuit paths including grain boundaries or defects may increase the diffusion coefficient of oxygen, which controlled the oxidation rate of the alloys. The dense and compact nature of the inner layer can also act as a diffusion barrier which may hurtle the further evolution of the oxide scales.

As the oxygen partial pressure increased, the diffusion of oxygen can be accelerated. Another continuous oxide layer appeared in the outer oxide region, which was found to be hematite Fe_2O_3 [16, 18, 20, 22]. Some studies [16] suggested that the formation of hematite phase can somehow benefit the corrosion resistance of the alloys by permeating the porous magnetite layer and blocking the diffusion. Therefore, it was found that the least weight gain can be achieved when the samples were exposed to SCW environment with intermediate dissolved oxygen values. An example of the oxide layer structures on the steel surface at two different dissolved oxygen contents are shown in Figure 1-7.

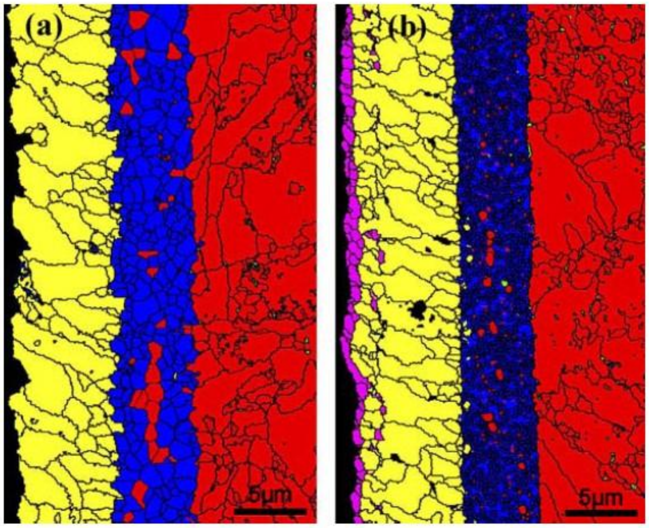

Figure 1-7. Cross-section EBSD scanning maps of SCW exposed HCM12A at 500 ℃ for 505 hours with: (a) 25 ppb dissolved oxygen and (b) 2000 ppb dissolved oxygen, where base metal, spinel, magnetite, and hematite are highlighted in red, blue, yellow, and magenta, respectively. Black areas are unindexed [22].

A few approaches were found to be effective to improve the performance of F-M steel in SCW environment. High temperature mechanical properties of the F-M steels can be remarkably enhanced by introducing fine dispersions of oxide particles into the matrix of the steels, which formed oxide dispersion strengthened (ODS) steels [21]. Recent studies also indicated that ODS steels, when proper designed and processed, can offer excellent corrosion resistance in air at temperatures up to 1000 ℃ [23, 24]. Therefore, ODS alloys show great potential to be applied as in-core or fuel cladding materials in SCWR. Moreover, it was found that the composition of the alloys can exert great influence on their chemical and mechanical properties; therefore the optimized SCW behavior can be expected by adjusting the alloying elements. Tan et al. [20] and Ampornrat et al. [16] suggested that F-M steels with a higher Cr content tended to have a lower oxidation rate; similar observation has also been reported on several ODS alloys [24, 25]. The effects of Al and Y alloying additions have been studied, and it was shown that Al had the tendency to suppress corrosion in SCW [24, 25] whereas the influence of Y was found to be of little significance [21, 25]. The addition of W can be detrimental to the corrosion performance [16]; however it can also increase the strength of the alloys [15]. Oxygen ion implantation conducted on T91 [18] and HT-9 [19] alloys has successfully reduced the thickness of the oxide layers by forming nano-sized precipitates which affected the preferred orientation and the growth texture of the oxide scales. The corrosion performance of the F-M alloys can also be enhanced by coated with proper materials, which will be elaborated in Section 1.2.6.

1.2.3 Austenitic stainless steels

Austenitic stainless steels are selected as the candidate fuel cladding and in-core materials in SCWR owing to their excellent corrosion and radiation resistance, low cost and higher strength at elevated temperature. However, comparing to F-M steels, they exhibit lower thermal conductivities and higher coefficients of thermal expansion, which may result in higher susceptibility to cracking or other mechanical failures [26].

The general corrosion behaviors of several austenitic steels, including 316L, 304, and N controlled 304L in SCW 480 ℃/25 MPa, were studied by Luo et al. [27]. Among the steels tested, 316L, which has a higher Cr and Ni content, exhibited the best corrosion resistance. Was et al. [28] reported the SCW behaviors of 304 and 316L stainless steels at temperatures ranged from 400 ℃ to 550 ℃. It was found that the weight changes of the samples were highly dependent on the temperature. A series of austenitic alloys (316, D9, NF709) were exposed to SCW environments at 500 ℃ and 600 ℃ to examine their corrosion performance [29]. Gravimetric test showed that at both temperatures, only limited oxidation can be observed for all the alloys tested. The study of the SCW corrosion and stress corrosion cracking performance of 304L and 316L conducted by Was et al. [30] indicated that under the same conditions 304L showed better oxidation resistance. Also, the oxide layers formed on 304L steel in non-deaerated water were found to be much thicker than those in deaerated water. Zhang et al. [31] conducted SCW test at 550 ℃/25 MPa with 2 ppm dissolved oxygen on austenitic steels TP347HFG and HR3C, and the results were compared with F-M steel P92 exposed to the same conditions. It was shown that the austenitic steels had a significantly lower oxidation rate than P92, and HR3C exhibited the best corrosion resistance.

The morphologies of the oxide scales formed on the austenitic stainless steels surface vary with the composition of the steels as well as the SCW test conditions. The oxides typically exhibited a two-layer structure [26, 28~30, 32~35], whereas in some studies a single oxide layer can been observed [27, 31, 36]. For dual layered oxide, the inner layer was enriched in Cr, and usually consisted of Cr_2O_3 mixed with Fe oxides and hydroxides. The outer layer, however, was depleted in Cr but contained significant amounts of Fe. At certain conditions (for instance, high dissolved oxygen content), only a layer of Fe/Cr oxides was presented on the alloy surface. The oxidation mechanism of the austenitic steels in SCW was quite similar with that of F-M steels, and the outer layer developed by the outward diffusion of cations whereas the inner layer grew by the inward diffusion of oxygen [28].

For austenitic steels exposed to SCW with high dissolved oxygen content, the formation of large flakes may occur on the outer oxide layer, which led to severe spallation [29]. Spallation can be evidently mitigated by grain boundary engineering (GBE) which helped to achieve a high volume fraction of low energy coincident site lattice boundaries [37, 38].

Studies indicated that the corrosion behaviors of austenitic steels in SCW environment can be affected dramatically by their alloying elements, and better corrosion can be witnessed for alloys comprising high content of Cr, Ni and Al [27, 39]. Furthermore, grain refinement was found to be effective to improve both corrosion performance and IGSCC resistance of austenitic steels, since a denser Cr_2O_3 layer tended to be formed on the alloys with smaller grain sizes, which can protect the alloys from further attacks [29, 35, 40].

1.2.4 Ni based alloys

Ni based alloys offer the advantages of superior corrosion resistance and mechanical properties resulting from solid solution and precipitate strengthening [41, 42]. Nevertheless, they also have the drawbacks of high cost and low phase stability, especially at high temperatures [43].

Comparing to F-M steels and austenitic steels, the performance of Ni based alloys in SCW are not extensively studied. Ma et al. [41] examined the feasibility of using Hastelloy C-276 as fuel cladding materials in SCWR. The results indicated that C-276 can provide sufficient high temperature strength and stability, which ensured their great potentials to be utilized in SCWR. The SCW response of alloy 625 was compared with that of 316 stainless steels [44]. It was shown that the corrosion and stress corrosion cracking resistance of Alloy 625 was both superior to 316 steels. The corrosion behaviors of four Ni based alloys in SCW containing hydrogen chloride at temperatures between 350 ℃ and 550 ℃ were investigated by Fujisawa et al. [45]. Their research showed that the weight loss of the alloys increased with higher hydrogen partial pressure, and alloy C-276 and MAT 21 exhibited better corrosion resistance than Inconel 625 and MC alloy. Tan et al. [42] investigated the corrosion resistance of Inconel 617, 625, and 718 in SCW at the temperatures range from 500 ℃ to 800 ℃. As the test carried on, both weight loss and weight gain can be observed for the alloys, and alloy 718 showed the worst SCW performance. The SCW tests at 500 ℃ and 25 MPa were conducted on C-276, Inconel 625, and Inconel X-750 by Zhang et al. [46]. The highest weight gain can be observed on alloy X-750, and the weight changes for all the samples were considerately small.

Cr and Mo were found to be the most crucial alloying elements of Ni based alloys, and studies showed that alloys with higher Cr and Mo content tended to have a better SCW corrosion resistance [42, 43, 45, 46]. Research conducted by Sugahara and Isobe [47] suggested that Ta addition can also be beneficial for the phase stability, toughness as well as the corrosion resistance of Ni based alloys exposed to SCW environment. Alloying elements Nb, Cu or W seemed to be detrimental [42, 47].

1.2.5 Other alloys

Zr based alloys are considered as candidate SCWR materials because of their low thermal absorption and high resistance to waterside corrosion [48]. However, whether they can withstand the severe corrosion at SCW environment is of great concerns. Also, it seems that the tensile strength at high temperatures (over 400 ℃) may also be deficient. SCW corrosion studies have been conducted on various Zr alloys [48, 49~51]. Studies suggested that the corrosion resistance of Zr based alloys was higher than most F-M alloys, whereas lower than austenitic steels [49, 50]. It was shown that the corrosion behavior of Zr based alloys was affected significantly by their compositions. Cr and Fe additions were found to be beneficial for the corrosion resistance of the alloys by contributing to the formation of a protective oxide layer on the alloy surface [48, 50, 51]. Among the Zr alloys tested, the Zr-Cr-Fe systems showed the potential to be utilized in SCWR, and they have been proven to be corrosion resistant in SCW at 500 ℃ for up to 400 days [49].

Ti based alloys also received attentions in the selection of SCWR candidate materials. At room temperature, Ti based alloys exhibit excellent mechanical properties. Nevertheless, their tensile strength can be decreased tremendously as the temperature mounting to 550 ℃ [52]. Kaneda et al. [53] reported that the corrosion resistance of Ti alloys was found to be between that of Ni based alloys and austenitic steels, and Cr, Mo and Zr can benefit the corrosion resistance of Ti alloys.

1.2.6 Ceramics

Ceramics are featured with excellent corrosion resistance, low thermal conductivity and high thermal stability, and thus show great potential to be used as coating or insulator materials in the SCWR.

Although it is generally acknowledged that ceramics are chemically inert and can hardly be corroded, the high temperature and pressure environment can also introduce substantial attack to the ceramic materials in SCW. The corrosion behaviors of various ceramic materials exposed to SCWO environment have been studied by Boukis et al. [54]. Their results demonstrated that in such oxidative environment, only a few Al_2O_3 and ZrO_2 based ceramics exhibited acceptable stabilities, whereas other ceramics either disintegrated or suffered enormous weight loss.

ZrO_2 has a thermal expansion coefficient close to most of the alloys, which can ensure adequate adhesion to the substrate when applied as coating materials [55]. Nevertheless, as can been seen from Figure 1-8, at low temperatures (below 1170 ℃) ZrO_2 has monoclinic structure which exhibits less satisfactory chemical and physical properties comparing to tetragonal phase [56, 57]. It was found that by adding certain amounts of foreign oxides, such as Y_2O_3, CeO_2 or MgO, the tetragonal phase can be stabilized at lower temperatures [58, 59].

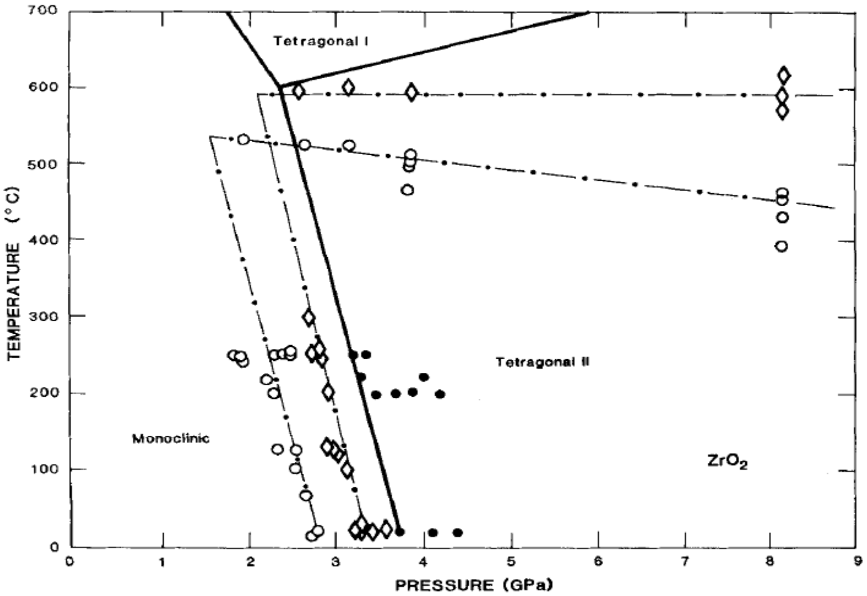

Figure 1-8. Phase diagram of ZrO_2 [56].

The SCW test of ZrO_2 coated carbon steel conducted by Guzonas et al. showed improved corrosion resistance after short time exposure at 455 ℃/29 MPa [60]. However, the ZrO_2 coating applied by the same method failed to provide any protection to 304 stainless steels. Y_2O_3 stabilized ZrO_2 coating has been prepared to protect 316L stainless steels from hot corrosion in molten chloride at 600 ℃ [61]. The coating was shown to be almost attack-free after 500 hours test. Orfino et al. [62] applied an Al_2O_3 added ZrO_2 coating on Zr alloys and examined the stability of the coating in SCW environment. The result showed that although the coating was efficient to reduce the corrosion resistance of the alloy at 500 ℃/25 MPa for up to 250 hours, it seemed that the protectiveness of the coating decreased as the exposure proceeded. However, ZrO_2 based ceramics possess undesirable high ion conductivity due to the additions of stability agents [63], which may restrict their applications in SCW environment.

Al_2O_3 ceramic is featured with excellent high temperature stability and hardness, as well as superior wear resistance [64, 65]. Schacht et al. [66] investigated the stability of Al_2O_3 in acidic solutions containing H_2SO_4, H_3PO_4 or HCl in SCW state at various temperatures. It was found that Al_2O_3 exhibited the highest weight loss in H_2SO_4 solution, followed by that in HCl and H_3PO_4. Moreover, it seemed that at higher temperatures, the degradation of the Al_2O_3 was predominantly attributed to the intergranular corrosion, rather the dissolution of the grains. Al_2O_3 has also been applied as coating materials to protect P91 steels from the corrosion attacks brought by SCW environment [67]. The study indicated that after exposure to SCW at 500 ℃/25 MPa for 500 hours, the P91 alloy with Al_2O_3 coating showed nine times reduced weight change comparing to the uncoated sample. Nevertheless, in both studies, it was reported that Al_2O_3 ceramic suffered severe attacked in subcritical water (from 250 ℃ to 300 ℃). As can be seen from Figure 1-9, the solubility of Al_2O_3 ceramic was found to be enormous in subcritical water, which may introduce severe attacks to the reactor when it starts up and operates in subcritical region if Al_2O_3 based ceramics are used in SCWR.

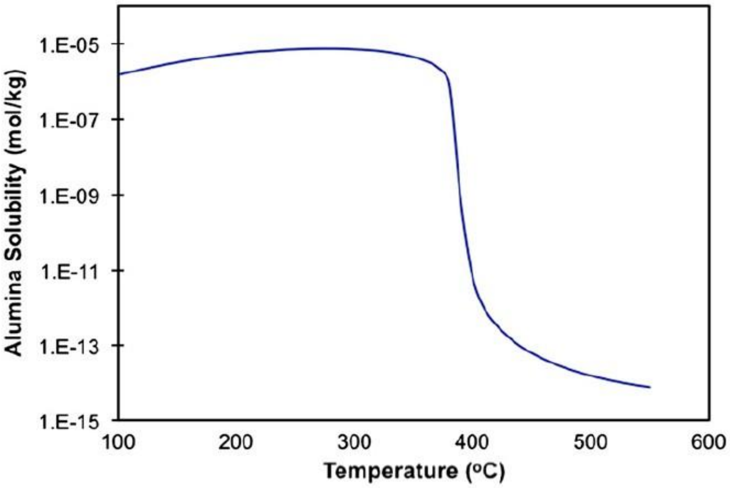

Figure 1-9. Theoretical solubility of Al_2O_3 as a function of temperature [67].

In Europe, Fe-Al slurry coatings were widely studied in supercritical steam turbine which is quite similar to supercritical water reactors. Mn containing aluminide was deposited on ferritic steels followed by a diffusion treatment at 700 ℃, which converted Al-rich coatings into FeAl and Fe_3Al and resulted in the formation of Cr-rich precipitates [68]. The achieved coating provided enhanced mechanical and chemical stability, therefore was regarded as one of the potential candidate materials to be used in SCW. Perez et al. [69] conducted corrosion test on Fe-Al slurry coated P92 steel in 80% water at 650 ℃. The results showed that after 150 hours the coating can provide 4 magnitude orders of less weight gain comparing to the uncoated materials. Similar coating applied on P91 substrate was found to be protective from wet corrosion at 650 ℃ which lasted for 78,000 hours [70]. Cracks were presented on the surface due to the thermal expansion mismatch but did not propagate into the steels. Although Fe-Al seemed to be promising for SCWR applications, more studies are imperative to further investigate their SCW behaviors.

Several studies have been conducted by Japanese on the stability of nitride ceramic coatings in SCW solutions. Different from oxide coatings, the protection provided by nitride coatings thrived from the oxidation of the nitride, which prevented further oxidation of the substrate. TiN, TiAlN and CrN films were applied on 304 stainless steel using Physical Vapor Deposition (PVD), and the steels were exposed to SCW solutions containing various ions between 600 ℃ ~850 ℃ [71]. All films were found to be protective in neutral and partially alkaline solutions, but unstable in acidic solutions. The formation of a $FeTiO_3$ ilmenite film was suggested to be the origin of the good corrosion resistance of TiN coated stainless steel at 600 ℃ and 100 MPa [72]. Korablov et al. [73] further investigated the hydrothermal corrosion of those three nitride films at 20 ℃~950 ℃ and 100 MPa, and they found that the temperature at which the film can withstand the exposure increased in the order of TiN (600 ℃), TiAlN (700 ℃)

to CrN (800 ℃). The long term protection of CrN films was induced by the formation of spinel at the temperatures up to 800 ℃ and of $Cr_{1.3}Fe_{0.7}O_3$ once the temperature exceeded 800 ℃.

Si based ceramics are also of great interest as the candidate SCW materials. Nagae et al. [74] examined the corrosion resistance of sialon, a ceramic containing Si, Al, O and N, in SCW at 450 ℃/45 MPa for 2~50 hours. After SCW test, a thin corroded layer containing Al_2O_3 and SiO_2 was discovered on the ceramics surface. It was also shown that α-sialon was more corrosion resistant than β- or α /β-sialon. Silicon carbide was reported to be very stable in SCW at 500 ℃; however the corrosion rate seemed to be higher at 360 ℃ [75]. Preferential attacks at the grain boundaries were observed for the ceramic after SCW test, and the corrosion mechanism was found to be the hydrolysis of the silica species. The SCW stability of silicon nitrite was investigated by Proverbio et al. [76]. Their results showed that silicon nitrite exhibited great weight loss between 400 ℃ and 500 ℃ owing to the high solubility of silica. The oxidation of silicon nitride was highly dependent on the impurities as well as the porosity of the ceramic.

1.3 Chromium oxide

Cr_2O_3 ceramic offers the advantages of high chemical stability, high wear resistance and low thermal conductivity, thus it has been applied as coating materials to prevent corrosion and wear in various harsh environments. The long term protectiveness of plasma sprayed Cr_2O_3 on several alloys in Cl-containing aqueous environments has been evaluated [77]. The results indicated that comparing to the uncoated alloys, Cr_2O_3 coating did not introduce substantial corrosion into the substrates. However, one major concern of the Cr_2O_3 coating is its poor adhesion with the substrate, which may result in the catastrophic attacks at the interface. To overcome this problem, an intermediate layer, usually NiCr, has been applied to enhance the adhesion. According to the study conducted by Li et al. [78], a 50NiCr intermediate layer can further improve the corrosion resistance of Cr_2O_3 coating, whereas 80NiCr layer deteriorated the performance of the coating. Zhu et al. [79] examined a novel Cr_2O_3 coating dispersed with CeO_2, and the results was compared with Cr_2O_3 coating without dispersion. It was shown that CeO_2 dispersions can induce a finer and more adherent coating, and they can also lower the oxidation rate of Cr_2O_3 coated mild steel remarkably.

Moreover, a protective Cr_2O_3 layer is commonly formed on the surface of Cr-containing steels and alloys when exposed to oxidative environment, and their corrosion resistance will be closely related to the stability of the Cr_2O_3 layer formed. It was found that a critical Cr content is necessary upon which the alloys can form a continuous Cr_2O_3 layer that is dense enough to offer oxidation protection. Boudin et al. [80] reported that for Ni-Cr alloy exposed to borate buffer solutions, the critical Cr value was found to be 15 at. %. Study conducted by Stott et al. [81] indicated that although protective Cr_2O_3 layer can be formed when the Cr content was in the range of 10%~20%, its establishment was quite slow and can be greatly affected by the transport of Cr to the surface. Therefore the formation of a dense Cr_2O_3 layer, which was less dependent on the Cr diffusion, can be ensured only when the Cr content exceeded 20%. Another influential factor on the formation of the Cr_2O_3 protective layer is the temperature. Riffald et al. [82] reported that the critical temperature for the formation of a protective Cr_2O_3 layer on 304 stainless steel surface should be around 1000 ℃. Alloying elements including Y, Si, and Al can promote the protectiveness of the Cr_2O_3 oxidation layer [82~85], whereas S was found to be detrimental since it can suppress the outward diffusion of Cr and retard the formation of Cr_2O_3 [86].

Figure 1-10 illustrated the pourbaix diagram for Cr in subcritical and supercritical environments obtained by theoretical calculations [87]. The diagrams indicated that in subcritical region, Cr can only be passivated when the pH was between 3 and 11, whereas in supercritical water the formation of a Cr_2O_3 passivation layer was possible for all pH ranges. Also, it was shown that in oxidizing conditions, Cr_2O_3 may be dissolved to form H_2CrO_4 or $HCrO_4^-$ species. However, little experimental work can be found in the literature on the stability of Cr_2O_3 in SCW environment.

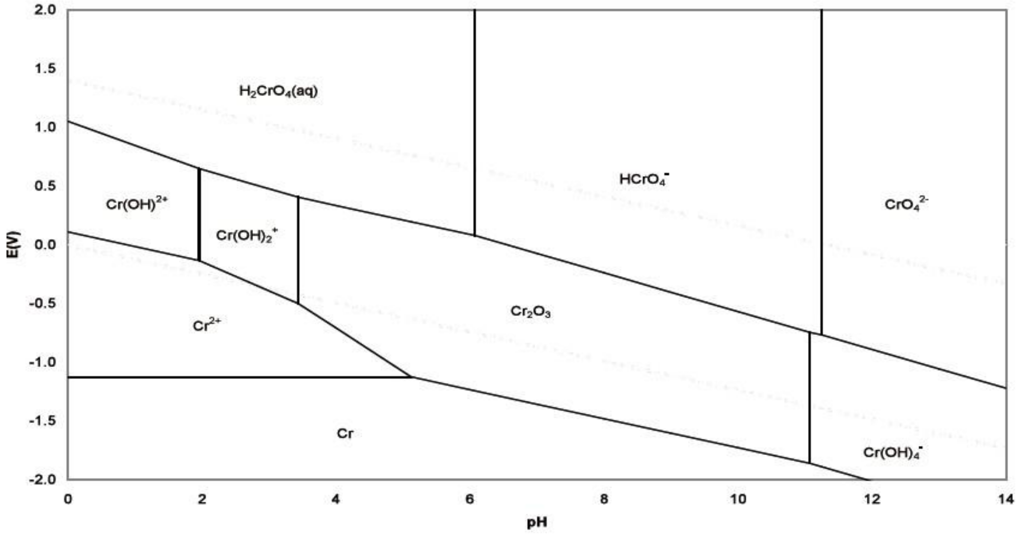

(a)

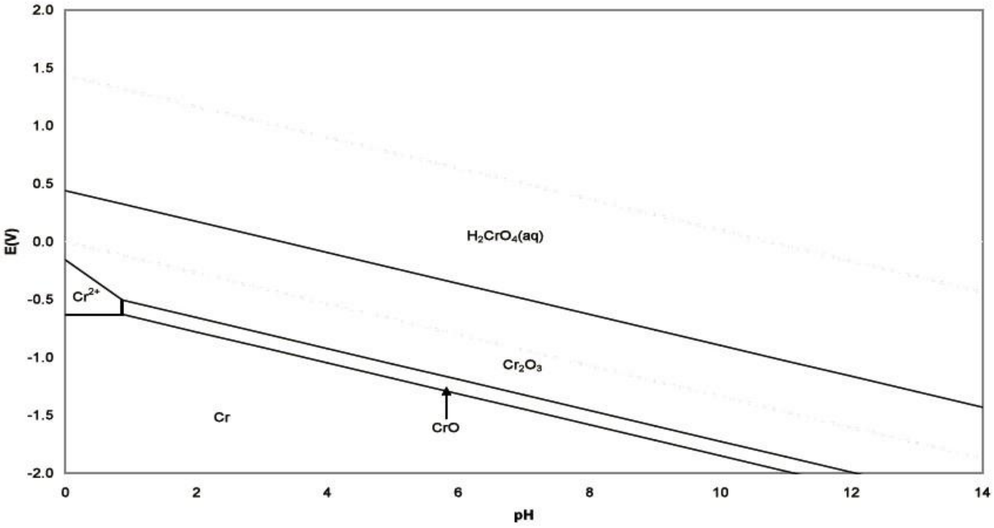

(b)

Figure 1-10. Pourbaix diagram of the Cr-H_2O system at: (a) 350 °C, 25 MPa, and 10^{-8} molar; (b) 400 °C, 25 MPa, and 10^{-8} molar [87].

Chapter 2 Research objectives

As indicated in Chapter 1, the study of the corrosion behaviors of Cr_2O_3 based ceramics in SCW condition can examine the feasibility of applying Cr_2O_3 as insulator materials or as protective coatings in SCWR. Moreover, it can also generate valuable knowledge benefiting the selection of proper Cr-containing steels and alloys applied in SCW environment. Nevertheless little is known on the corrosion mechanisms of Cr_2O_3 based ceramics in SCW conditions as well as its responses to corrosion after added by various oxide additions. The objectives of the current study are as follows:

1. To investigate the corrosion mechanism of Cr_2O_3 based ceramics in SCW environments;

2. To determine whether and how grain size and dissolved oxygen content affect the corrosion behaviors of Cr_2O_3 based ceramics in SCW;

3. To examine the effect of oxide additions, including MgO, CeO_2 and SiO_2, on the stabilities of Cr_2O_3 based ceramics in SCW conditions.

Chapter 3 Experimental

3.1 Preparation of Cr_2O_3 based ceramics

Details of ceramic powders utilized as starting materials in this study are listed in Table 3-1. It can be seen from the table that three Cr_2O_3 powders were used. MgO, CeO_2 and SiO_2 were selected as oxide additions which were mixed into Cr_2O_3 powders with mass percentages of 1%, 5% and 8%, respectively. Ball milling treatment with alumina beads was conducted at room temperature for 24 hours in order to achieve uniformly mixed compositions.

Table 3-1. The ceramic powders used in the current study.

Group No.	Composition	Purity	Particle size	Supplier
1	Cr_2O_3	98%	100 mesh	American Elements
2	Cr_2O_3	98%	325 mesh	Alfa Aesar
3	Cr_2O_3	98%	50 μm	Sigma-Aldrich
4	MgO	96%	325 mesh	Alfa Aesar
5	CeO_2	99.5%	325 mesh	Alfa Aesar
6	SiO_2	99.5%	325 mesh	Alfa Aesar

The oxide powders were then compressed to form disk-shaped samples under a pressure of 70 MPa using a cylindrical mold with a diameter of 16 mm. The obtained coupons were sintered in a chamber furnace (Lindberg/Blue M, Tech-

Met Canada) at 1200 ℃ for 15 hours. After sintering, the ceramics were cut and polished into 10 mm×5 mm×2 mm rectangular-shaped samples, which were thereafter ultrasonically cleaned in ethanol alcohol bath. Typical appearance of samples after compressing or after cleaning is presented in Figure 3-1.

(a) (b)

Figure 3-1. The Cr_2O_3 based ceramic sample: (a) as compressed; (b) after sintering and sectioning into coupons for SCW exposure.

3.2 SCW test

All SCW tests were at 650 ℃ and 25 MPa, and the durations of the tests were 200, 400 and 600 hours. Three tests were repeated for each condition and the results were averaged. The tests were conducted using the static reactor as illustrated in Figure 3-2.

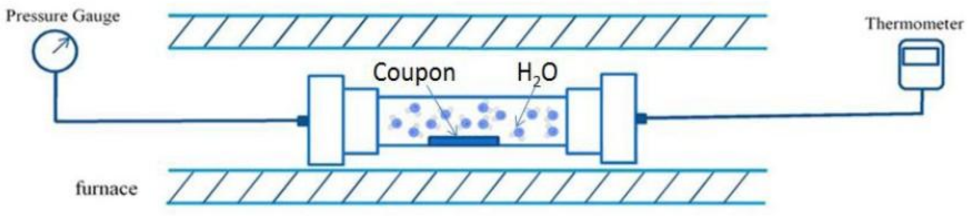

Figure 3-2. Schematic of the SCW test reactor adopted in the current study.

The samples were put into capsules (with a length of 65 mm) cut from Inconel 625 tube with an outer diameter of 9.53 mm and a wall thickness of 1.65 mm. The volume of the capsules V_{cap} was calculated as follow:

$$V_{cap} = \frac{1}{4}\pi d_{in}^{2} L \tag{1}$$

where d_{in} and L refer to the inner diameter and the length of the capsules respectively. In order to maintain the desired pressure inside the capsules, controlled amount of deionized water or 30% H_2O_2 was added into the capsules. As the temperature increases, the hydrolysis of the H_2O_2 would take place:

$$H_2O_2 \rightarrow H_2O + O_2 \tag{2}$$

The volume of the liquid needed was calculated based on the isobaric properties for water at 25 MPa listed in Table 3-2. According to the table, the density of the water at 650 ℃/25 MPa is 0.064810 g/ml. Therefore, the volume of the liquid V_{liquid} needed can be determined:

$$V_{liquid} = \begin{cases} \dfrac{0.064810\,V_{cap}}{\rho_{H_2O}} & \text{when added with } H_2O \\ \dfrac{0.064810\,V_{cap}}{(70\%+30\%\times\frac{18}{34})\rho_{30\%H_2O_2}} & \text{when added with } H_2O_2 \end{cases} \tag{3}$$

The value of V_{cap} can be obtained by equation (1). ρ_{H_2O} and $\rho_{H_2O_2}$ represent the density of water and of 30% H_2O_2 at 25 ℃/1 atm, and were determined to be 1.00 g/ml and 1.11 g/ml respectively.

Table 3-2. Isobaric properties for water at 25 MPa [88].

Temperature(℃)	Pressure(MPa)	Density(g/ml)	Volume(ml/g)
500	25	0.089744	11.143
550	25	0.078517	12.736
600	25	0.070720	14.140
650	**25**	**0.064810**	**15.430**
700	25	0.060084	16.643

In this study, no measures have been taken to purge air out of the capsules before sealing. Therefore, the dissolved oxygen content p_{O_2} inside the capsules can be acquired by the following equations:

$$p_{O_2} = \left\{\begin{matrix} \dfrac{21\%\rho_{O_2}(V_{cap} - V_{liquid})}{\rho_{H_2O}V_{liquid} + \rho_{air}(V_{cap} - V_{liquid})} & \text{when added with } H_2O \\ \dfrac{21\%\rho_{O_2}(V_{cap} - V_{liquid}) + \frac{30\%\rho_{H_2O_2}V_{liquid} \times 32}{34\times 2}}{\rho_{H_2O_2}V_{liquid} + \rho_{air}(V_{cap} - V_{liquid})} & \text{when added with } H_2O_2 \end{matrix}\right\} \quad (4)$$

In equation 4, the density of oxygen (ρ_{O2}) and air (ρ_{air}) at room temperature were 1.31 g/l and 1.21 g/l respectively. According to the equation, the dissolved oxygen content was calculated to be roughly 3920 ppm when added with deionized water and 168295 ppm when added with 30% H_2O_2. After adding liquid, the capsules were thereafter sealed by 3/8 316 stainless steel caps lubricated with silver colloid. One of the sealed capsules is shown in Figure 3-3.

Figure 3-3. The sealed capsule with ceramic sample inside.

The stabilities of the Cr_2O_3 based ceramics were determined by weight changes after the SCW exposure, which were calculated based on the following equation:

$$\text{Weight change, \%} = \frac{\text{Weight}_{\text{after}} - \text{Weight}_{\text{before}}}{\text{Weight}_{\text{before}}} \times 100\% \qquad (5)$$

The weights of the samples before and after SCW test were acquired by a Mettler Toledo XS105 balance with a detection limit of 0.00001 g.

3.3 XRD analysis

As one of the non-destructive detection techniques, X-ray diffraction (XRD) analysis can provide valuable information regarding to the crystal structure of the materials. According to Bragg's law [89], the X-ray scattered pattern is linked with the crystal properties of the materials by the following equation:

$$2\mathrm{d} \sin \theta = \mathrm{n}\lambda \qquad (6)$$

where *d* refers to the inter-planar distance for the crystal lattice of the detected material; θ represents the diffraction angle and λ is the wavelength of the X-ray; n is an integer reflecting the series of diffraction. Bragg's law revels that by capturing the scattered intensity as a function of diffraction angles, the crystal properties of the material can be obtained.

In the current study, XRD patterns of the ceramics were recorded to determine the crystalline properties of the Cr_2O_3 based ceramics by a Rigaku Geigerflex 2173 X-ray diffraction equipment with Cu K_α radiation, with a scanning rate of 3 degree/min from 10 to 110 degree. The obtained diffraction patterns were analyzed by Jade software.

3.4 SEM analysis

Scanning electron microscopy (SEM) is widely used to examine the morphology and composition of the sample surface by scanning the sample with electron beams and collecting the signal generated from the sample surface as a response of the electrons. Equipped with an energy-dispersive X-ray (EDX) spectroscope, it also provides quantitative characterization of elemental distribution at the surface.

Two SEM facilities were employed in the current study, which were JEOL (JSM-6301 FXV) field emission SEM with an acceleration voltage of 5 eV and ZEISS (EVO –MA 15) SEM with an acceleration voltage of 20 eV. Prior to the test, samples were coated with gold in order to increase the electrical conductivity of the tested surface.

The grain size of the materials can be estimated based on the SEM images using the intercept method. Six lines (three vertical and three parallel) with identical length were drawn through the SEM images, and the amounts of grains intercepted by the lines were calculated. The average grain size can be obtained using the below equation:

$$\text{Grain size} = \frac{1}{6}\sum_{0}^{6}\frac{\mathrm{L}}{\mathrm{n_i M}} \tag{7}$$

where L is the length of the lines, n_i the number of grains intercepted, and M represents the liner magnification of the images.

3.5 Mass spectrum (MS) test

As a plot of signal intensity vs. mass-to-charge ratio of the element, MS enables accurate determination of the concentration of certain elements in a solution. After SCW test, the remaining water liquid was analyzed using an inductively coupled plasma mass spectrometer (ICP-MS) Perkin Elmer Elan 6000, to quantify the element concentration. The test results were normalized in order to minimize the error induced by the weight differences between the samples.

3.6 XPS analysis

By attacking the sample with X-ray and measuring the number of electrons escaped at the surface as a function of binding energy, X-ray photoelectron spectroscopy (XPS) can offer information related to the composition, uniformity, and chemical or electronic states of the material being examined.

XPS test was conducted in this study by a Kratos Axis 165 X-ray Photoelectron Spectrometer. The obtained spectrums were examined using CasaXPS software.

C 1s (286.4 eV) was selected as the standard reference to eliminate the effect of peak shift.

Chapter 4 Results and discussions

4.1 Stability of pure Cr_2O_3 ceramic in SCW environment

4.1.1 Corrosion behavior of Cr_2O_3 in SCW

According to the poubaix diagram of Cr in SCW environment (Figure 1-10 b), Cr_2O_3 may be oxidized by the following reaction:

$$\mathrm{Cr_2O_3 + O_2 + H_2O \xrightarrow{SCW} H_2CrO_4} \quad (8)$$

Since H_2CrO_4 is soluble to water, Cr_2O_3 may suffer weight loss due to the formation of Cr^{6+} species through the above reaction.

To verify the occurrence of the above reaction, the stability of pure Cr_2O_3 ceramic synthesized using #2 Cr_2O_3 oxide powder listed in Table 3-1 (98%, 325 mesh), was examined first in 650 ℃/25 MPa SCW. The surface morphologies of the Cr_2O_3 sample after sintering are presented in Figure 4-1. It can be seen that the ceramics manufactured by the current sintering method (1200 ℃ in air for 15 hours) were rough and porous with nano-sized particles chemically bonded with each other. Under high magnification (Figure 4-1 b), the Cr_2O_3 ceramic particles showed crystalline features, indicating that each particle can be considered to be one grain.

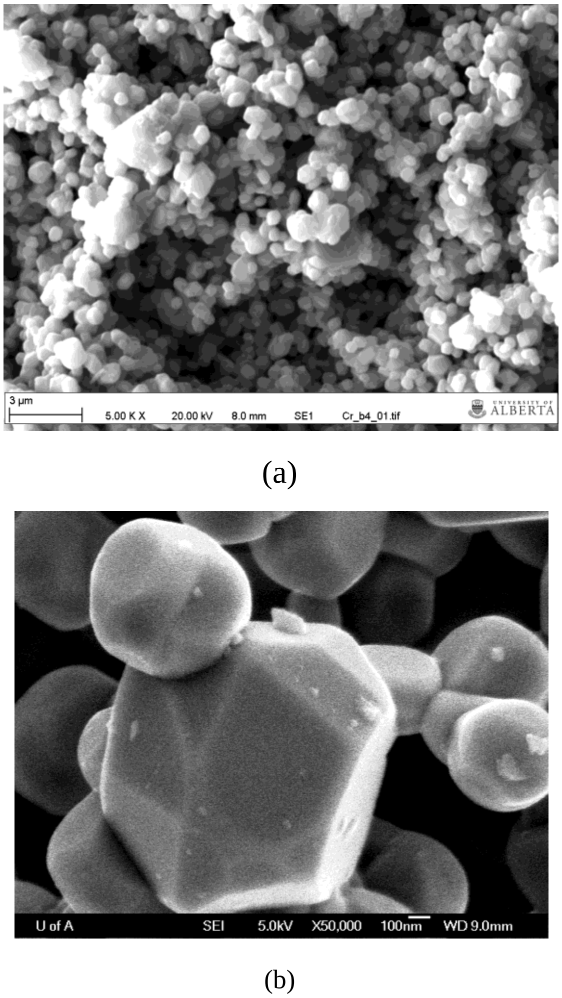

(a)

(b)

Figure 4-1. Surface morphologies of Cr_2O_3 ceramic at a magnification of: (a) 5000; (b) 50000.

The weight changes of Cr_2O_3 ceramic after exposed to SCW at 650 ℃/25 MPa for up to 600 hours are shown in Figure 4-2. The result demonstrated that in SCW environment, weight loss can be observed for Cr_2O_3, which increased with longer exposure time.

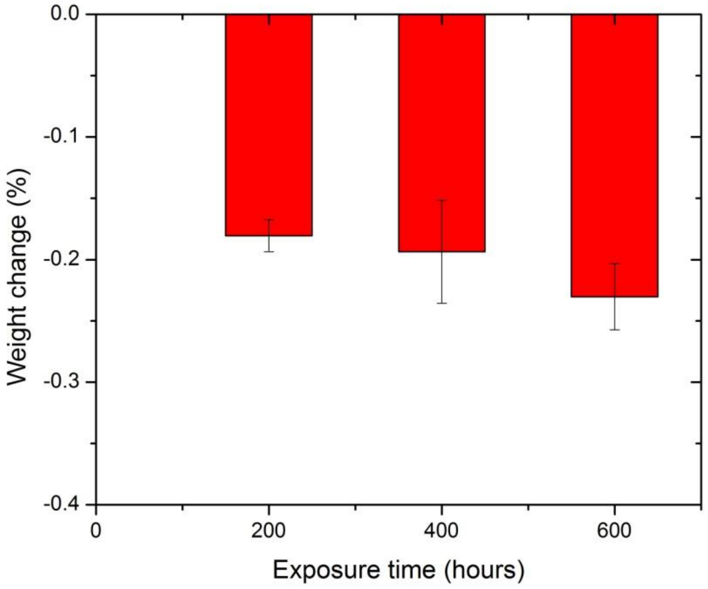

Figure 4-2. Weight changes of Cr_2O_3 ceramic exposed to SCW at 650 ℃/25 MPa for 200, 400 and 600 hours.

Mass spectrum analysis on the water after SCW test traced the presence of dissolved Cr ions, as can be seen in Figure 4-3. Nevertheless, XPS test conducted on the frozen water failed to show any Cr peaks, which may be due to the detection limit of the XPS equipment since the Cr concentrations in the water, as detected by mass spectrum tests, were overall quite small (less than 12 ppm per mass unit). When added with deionized water, the dissolved oxygen content inside the capsules was quite low (about 3920 ppm), which may be insufficient to produce significant amount of dissolved Cr.

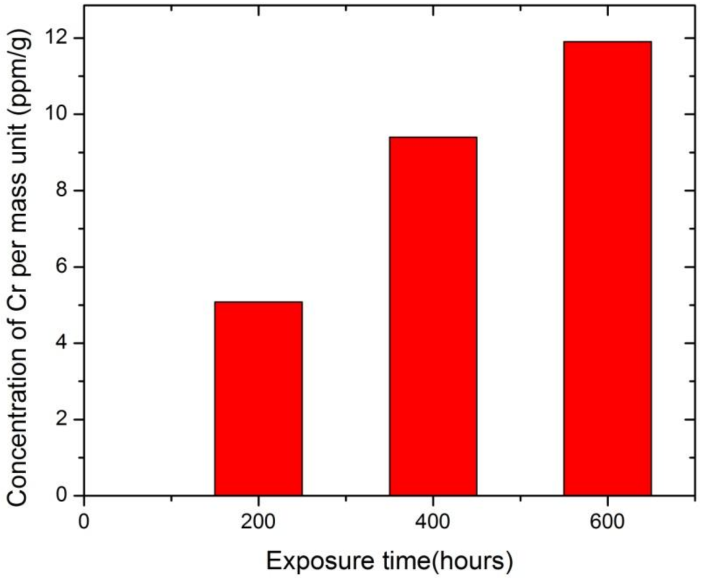

Figure 4-3. Concentrations of Cr in the water remained in the tube after Cr_2O_3 was exposed to SCW at 650 ℃/25 MPa for 200, 400, and 600 hours. (The results were normalized by the weight of bulk ceramics.)

4.1.2 Effect of dissolved oxygen content

In order to increase the dissolved oxygen content, 30% H_2O_2 solution, instead of deionized water, was added into the capsules before sealing. As a consequence of the hydrolysis of the H_2O_2 which formed H_2O and O_2, the oxygen content inside the capsules can be increased to over 160000 ppm.

Figure 4-4 illustrates the weight changes of Cr_2O_3 ceramic exposed to SCW containing 30% H_2O_2 at 650 ℃/25 MPa for up to 600 hours. Comparing to that in deionized water, weight gain instead of weight loss was observed, which increased as the exposure time became longer.

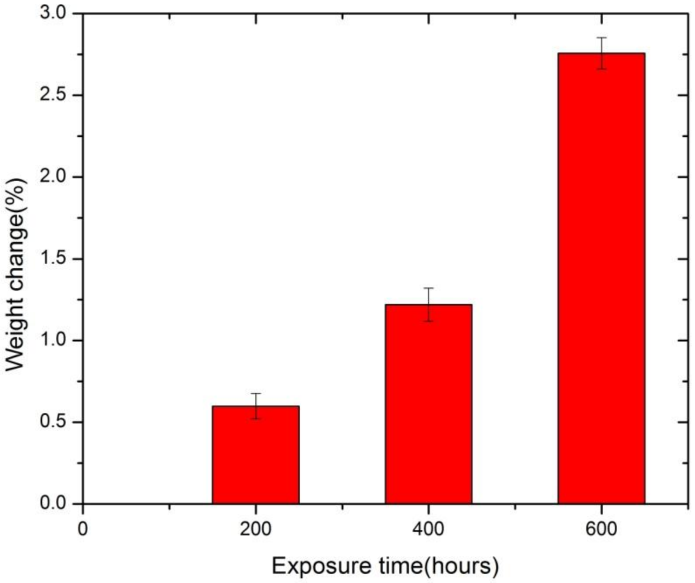

Figure 4-4. Weight changes of Cr_2O_3 ceramic exposed to SCW at 650 ℃/25 MPa with 30% H_2O_2 for 200, 400 and 600 hours.

It can be seen from the mass spectrum test results shown in Figure 4-5 that, as the dissolved oxygen content became higher, the concentration of Cr remained in the water increased tremendously. However, the capsules employed in this study were cut from Inconel 625 tube which contains 20~30 wt. % Cr alloying additions. Therefore, other than the dissolution of the Cr_2O_3, the corrosion of the capsule tubes may also contribute to the dissolved Cr as detected by mass spectrum tests. In order to quantify the dissolution rate of the Cr from the Ni alloy tube, capsules without ceramics samples were exposed to SCW under the same conditions, and the mass spectrum tests were conducted on the water after the tests. The results showed that the concentration rate of Cr was less than 1 ppm for capsules without samples, which was considerably small comparing with the results shown in Figure 4-5 (200 ppm to 400 ppm before normalization). This result, which is in consistent with other results obtained in our group [90], implied that in SCW with high dissolved oxygen content the dissolution of Cr from the capsule tube was marginal and thus can be omitted. Therefore the dissolved Cr shown in Figure 4-5 mainly resulted from the corrosion of the bulk ceramics.

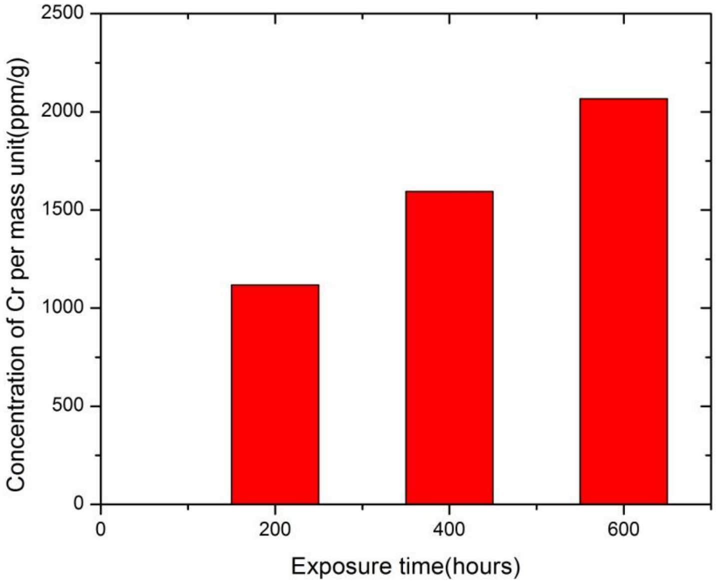

Figure 4-5. Concentrations of Cr in the water remained in the tube after Cr_2O_3 was exposed to SCW with 30% H_2O_2 at 650 ℃/25 MPa for 200, 400, and 600 hours. (The results were normalized by the weight of bulk ceramics.)

The Cr 2p photoelectron spectra obtained by XPS technique on the water after SCW exposure for 200 hours is displayed in Figure 4-6. The peak positions were normalized using C 1s (284.6 eV) as a standard reference, and the results are listed in Table 4-1 and they are compared with data found in the literature.

According to Table 4-1, the Cr ions remained in the water were identified as Cr^{6+} species, indicating that Cr_2O_3 based ceramics can be oxidized into soluble H_2CrO_4 in SCW environment. This confirms the results reported previously in our group [90].

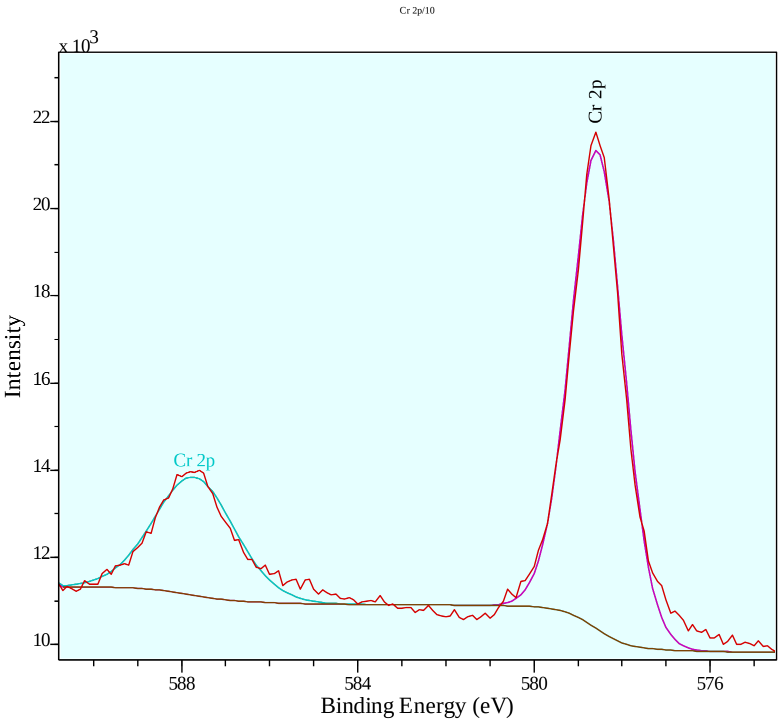

Figure 4-6. Cr 2p spectra of the water remained in the tube after Cr_2O_3 was exposed to SCW with 30% H_2O_2 at 650 ℃/25 MPa for 200 hours.

Table 4-1. The binding energies obtained in the current study compared with data in the literatures.

		Cr $2p_{3/2}$/eV	Cr $2p_{1/2}$/eV
Current study		588.9	579.7
Ref. [91]	Cr III	586.4	576.6
	Cr VI	588.7	579.7
Ref. [92]	Cr III	583.3	576.8
	Cr VI	586.7	579.3

Despite that large amounts of Cr_2O_3 have been dissolved into the water after SCW exposure, a weight gain, instead of weight loss, was recorded. To rationalize the above contradictory, SEM analysis was conducted on the sample after exposure for 200 hours in SCW, and the result is shown in Figure 4-7.

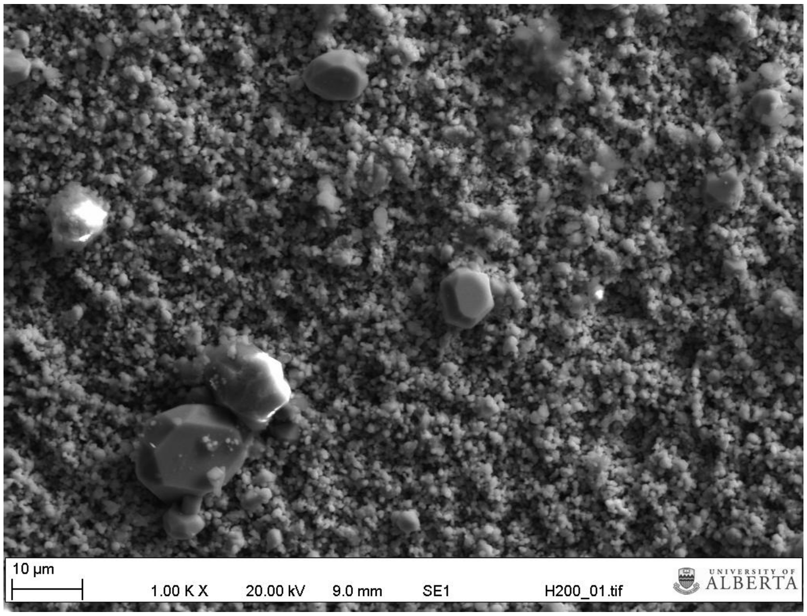

Figure 4-7. Surface morphology of Cr_2O_3 after exposure for 200 hours in SCW with 30% H_2O_2 at 650 ℃/25 MPa.

It can be seen in Fig. 4-7 that crystalline particles with diameters between 5 µm and 10 µm were observed to be deposited on the sample surface after exposure. EDX analysis of these particles is shown in Figure 4-8. Both Ca and Mo were detected in addition to Cr and O. XRD analysis of the sample after exposure is shown in Figure 4-9, and the detection of $CaMoO_4$ further confirms the presence of Ca and Mo, most likely from the crystalline particles found on the surface after exposure.

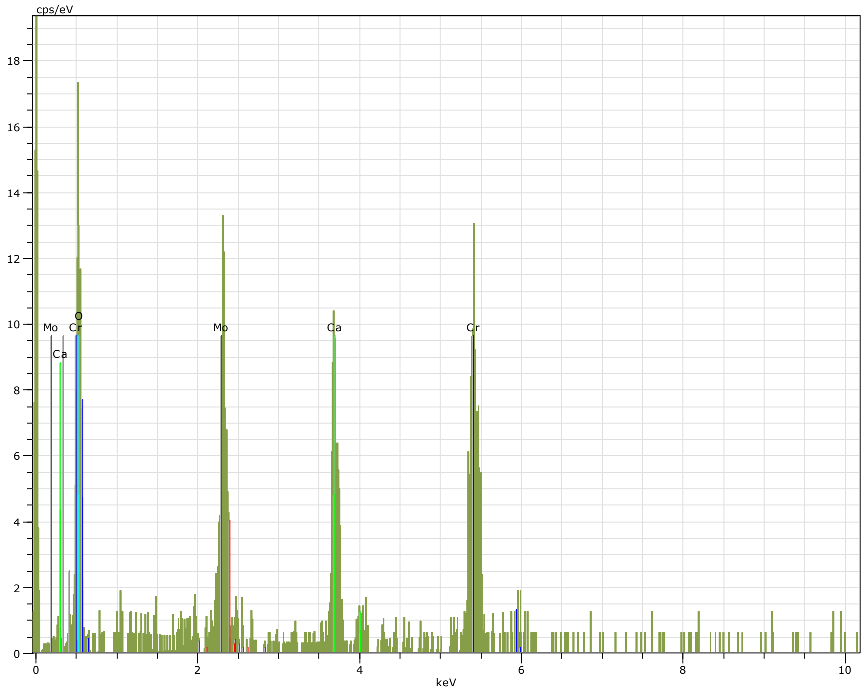

Figure 4-8. EDX test result on the large particles observed in Figure 4-7.

The capsule utilized in the current study was fabricated from Inconel 625 which contains 8%~10% Mo. Therefore, it is highly likely that the SCW with high oxygen level had also caused severe oxidation of the capsule, which led to the dissolution of Mo into Mo^{6+}. The latter further reacted with CaO, which is known as one of the most common impurities in metal oxides, to form $CaMoO_4$, when the reactor was cooled to room temperature. This has caused an increase of weight despite that substantial weight loss due to dissolution of Cr_2O_3 into soluble Cr^{6+} has occurred.

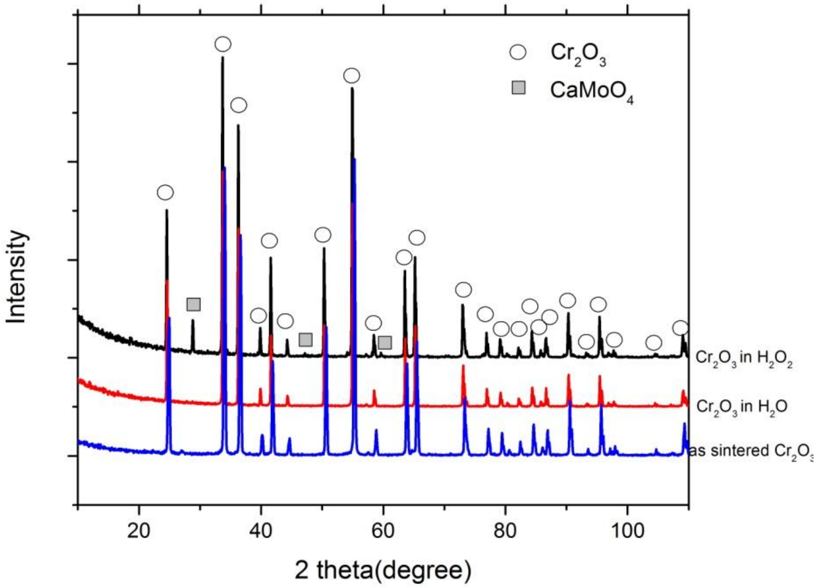

Figure 4-9. XRD patterns of Cr_2O_3 ceramics exposed to SCW at 650 ℃/25 MPa with deionized water or 30% H_2O_2 for 600 hours compared with as sintered Cr_2O_3.

4.1.3 Effect of grain size

For the purpose of examining the effect of grain size of Cr_2O_3 ceramic on its stability in SCW, three types of Cr_2O_3 powders with different particle sizes, as listed in Table 3-1 as No. 1~3, were employed as starting materials. Figure 4-10 shows the surface morphologies of the three types of Cr_2O_3 ceramics after sintering at 1200 ℃ for 15 hours. The grain sizes of those samples were determined based on Figure 4-10 using the line interception method, and the results obtained are shown in Table 4-2.

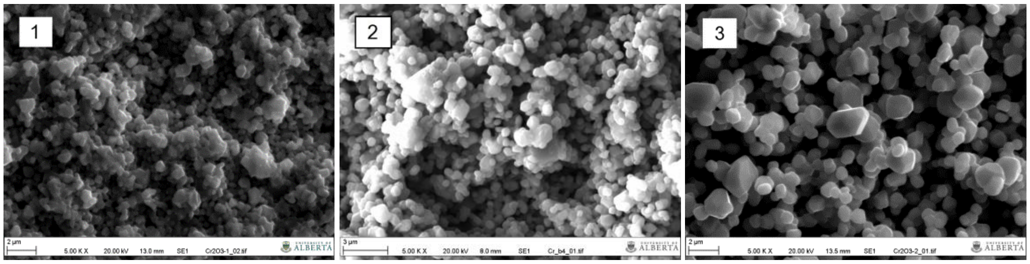

Figure 4-10. Surface morphologies of Cr_2O_3 ceramics with various grain sizes.

Table 4-2. Estimated average grain sizes of Cr_2O_3 ceramics.

Sample group	Average grain size(nm)
1	372.6 ±16.5
2	453.5 ±14.4
3	719.9 ±16.3

SCW tests of the samples listed in Table 4-2 were conducted at 650 ℃/25 MPa with deionized water for 200, 400 and 600 hours, respectively. Figure 4-11 presents the weight changes of the Cr_2O_3 ceramics as a function of their grain sizes. It can be seen that Cr_2O_3 ceramics with smaller grain size tended to have poorer stability in SCW. As average grain size decreases, the relative fraction of grain boundaries increases. Since grain boundaries are short paths of oxygen diffusion and at higher energy state, higher rate of Cr_2O_3 dissolution can be expected for samples with smaller grain sizes.

It can also be observed from Figure 4-11 that the dependence of weight changes on exposure time was also affected by the grain size. The variation of weight changes with testing time decreased as the grain size of the Cr_2O_3 became larger. This is because for Cr_2O_3 with smaller grains, higher value of grain boundary area tended to enlarge the differences induced by the various exposure hours, whereas as the grain size increase, this enlargement effect was reduced. However, it is difficult to explain why for the Cr_2O_3 with the smallest grain size, the largest weight loss was observed after exposure for 200 hours.

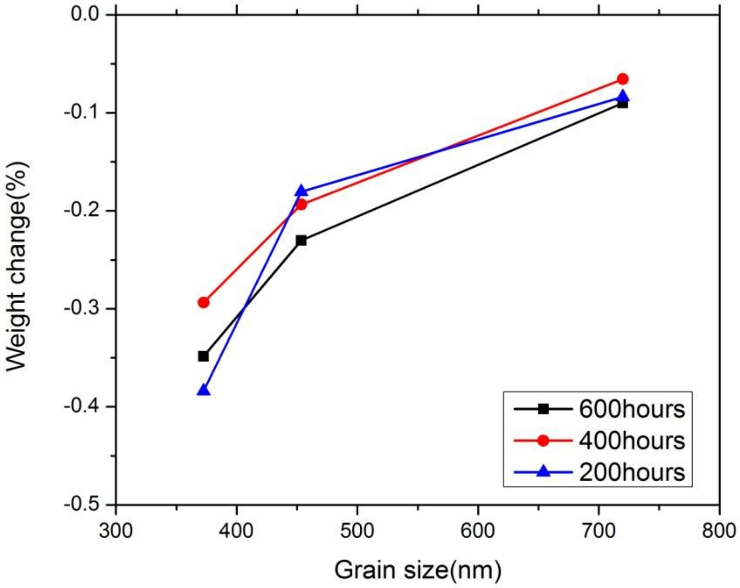

Figure 4-11. Weight changes of 3 groups of Cr_2O_3 ceramics exposed to SCW at 650 ℃/25 MPa for 200, 400 and 600 hours.

4.1.4 Summary

In this section, the stability of pure Cr_2O_3 in SCW environment was examined. It was found that Cr_2O_3 can be dissolved into species soluble to SCW, especially when the oxygen content in SCW is high. XPS test conducted on the water sample after SCW test indicated the presence of Cr^{6+}, implying that the degradation of Cr_2O_3 in SCW mainly resulted from its reaction with water and oxygen to form H_2CrO_4 acid. It was also found that the Cr_2O_3 ceramic with larger grains tended to have higher stability in SCW in terms of weight loss. This may result from the relative smaller fraction of grain boundaries, since the dissolution of Cr is more preferentially to take place at grain boundaries.

4.2 Effects of oxide additions on the stabilities of Cr_2O_3 based ceramics in SCW

Minor amounts of oxide additives (less than 10 wt. %) can exert significant impact on the properties of ceramic materials, including density, phase stability, strength and flexibility as well as corrosion resistance. The stability of Y_2O_3 doped Cr_2O_3 ceramics in SCW environment has been investigated previously [90]. The study showed that addition of 5 wt. % Y_2O_3 can be beneficial to the stability of Cr_2O_3 based ceramics. In the current study, three oxides, MgO, CeO_2 and SiO_2 were selected to examine their influences on the stability of Cr_2O_3 in SCW condition. No. 2 Cr_2O_3 powder with a mesh size of 325, as listed in Table 3-1, was used to be mixed with other oxide additives. The mixtures were ball milled before sintering using the same parameters as used for sintering pure Cr_2O_3. Pure

Cr_2O_3 was also ball milled in order to nullify effects of ball milling process (if any) on the particle sizes of Cr_2O_3 powders. The average particle sizes of all samples after ball milling were determined to be in the range of 200~250 nm by SEM observation.

MgO has been commonly added into oxide powders prior to sintering process as a sintering aid, which can make ceramic materials being sintered become denser and possess smaller grain sizes [93]. It was also found that MgO addition can improve the corrosion resistance of Al_2O_3 in aqueous hydrofluoric acid due to its segregation to the grain boundaries [94]. It was expected that the addition of MgO would improve the stability of Cr_2O_3 in SCW environment as well. Rare earth element Ce, like Y, is one of the widely used reactive elements [95]. The introduction of reactive elements into steels was shown to be beneficial to the formation of a more adherent and protective oxide layer without spallation [96]. Yet little is known about the influence of Ce addition on the corrosion of bulk Cr_2O_3 ceramics. The role of SiO_2 in high temperature oxidation was found to be controversial. 4% Si addition to the Fe-14Cr-14Ni steels can promote the formation of an inner SiO_2 layer which was shown to be effective in blocking the diffusion of Fe and in decreasing the oxidation rate remarkably [97]. Nonetheless, silica film formed at the grain boundaries can deteriorate the resistance to wet corrosion of Al_2O_3 based ceramics [98]. Since SiO_2 is present in most of the commercial oxide powders as impurity, their stability as well as their effect on the stability of other oxides is of interest and needs to be investigated.

4.2.1 Effect of MgO addition

Figure 4-12 shows a comparison of the XRD patterns of the MgO added Cr_2O_3 ceramics with that of pure Cr_2O_3 ceramic. It can be seen that besides the Cr_2O_3 phase, $MgCr_2O_4$ spinel phase has been formed, which is in accordance with the phase diagram of the MgO-Cr_2O_3 system shown in Figure 4-13.

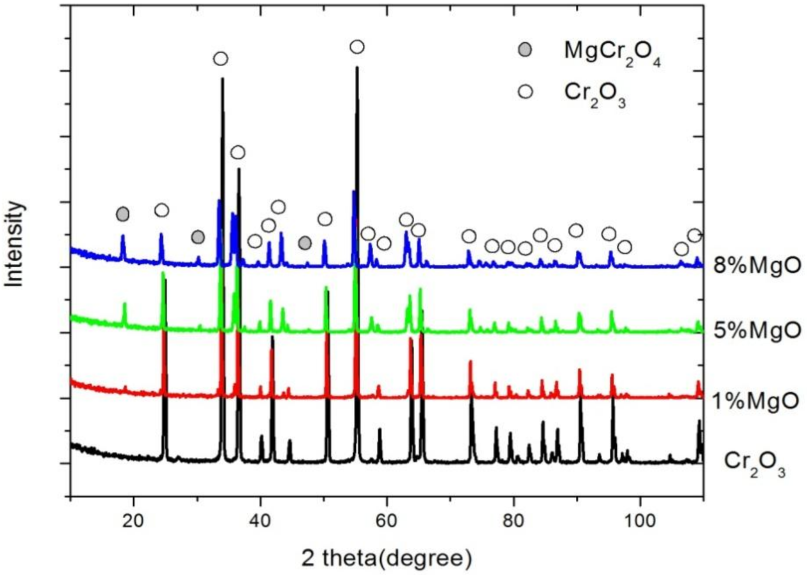

Figure 4-12. XRD patterns of MgO added Cr_2O_3 ceramics compared with that of pure Cr_2O_3.

From the surface morphologies of MgO added Cr_2O_3 after sintering (Figure 4-14), it can be seen that the grain sizes of the ceramics can be affected by the addition of MgO. The average grain sizes of the ceramics were determined based on the images in Figure 4-14 and are listed in Table 4-3.

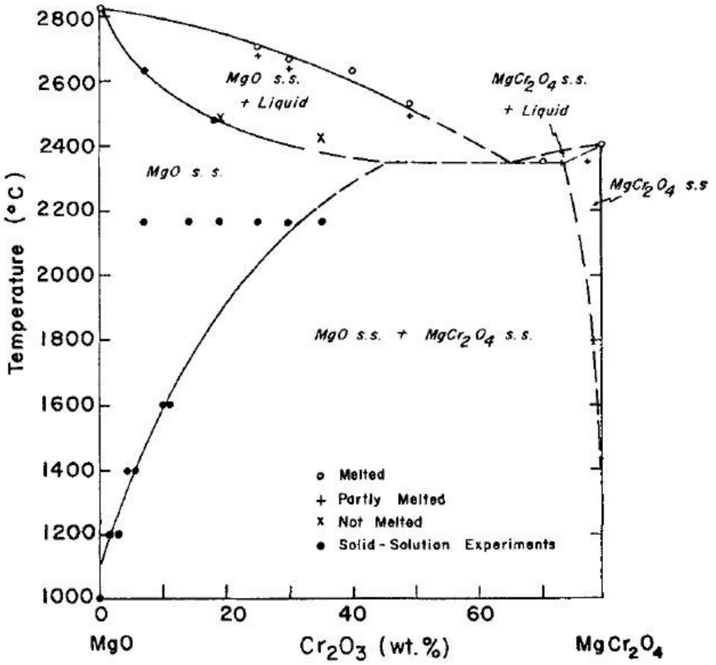

Figure 4-13. Phase diagram of Cr_2O_3-MgO binary system [99].

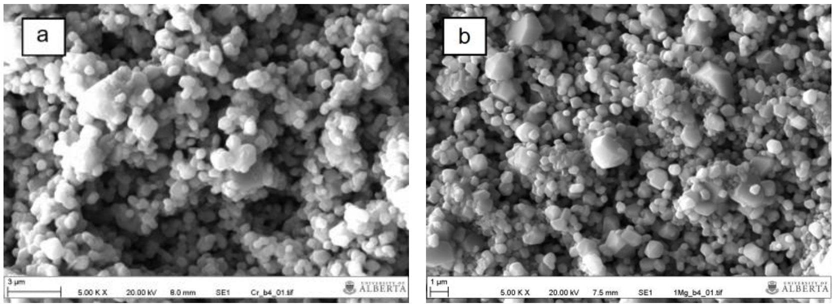

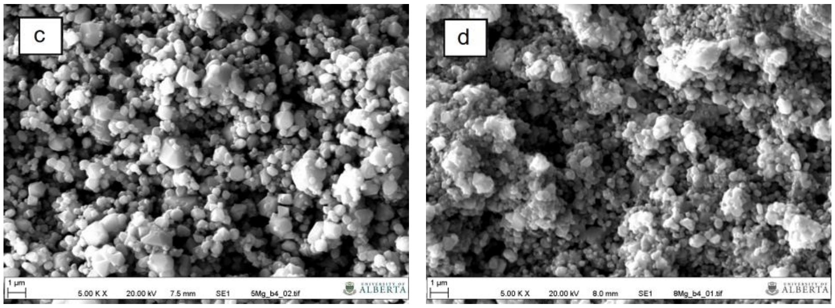

Figure 4-14. Surface morphologies of: (a) pure Cr_2O_3; (b) 1 wt. % MgO added Cr_2O_3; (c) 5 wt. % MgO added Cr_2O_3 and (d) 8 wt. % MgO added Cr_2O_3.

Table 4-3. Estimated average grain sizes of Cr_2O_3 based ceramics with MgO additions.

Sample	Average grain size(nm)
Cr_2O_3	453.5 ±14.4
Cr_2O_3+1 wt. % MgO	452.7 ±14.5
Cr_2O_3+5 wt. % MgO	449.2 ±17.3
Cr_2O_3+8 wt. % MgO	351.7 ±11.3

The grain size of MgO added Cr_2O_3 was barely affected by MgO addition until the additive content reached 8 wt. %, at which the grain size was found to be much smaller. The grain refinement phenomenon caused by adding MgO can be attributed to the grain boundary pinning effect [100], whereby the dispersed impurity particles act as obstacles to hinder the migration of grain boundary during the sintering process. It was predicted that grains would stop growing once their mean radius reached a critical value governed by the following equation [101]:

$$\overline{R}_{lim} = K\frac{r}{f_V^b} \tag{9}$$

where *r* represents the particle radius, f_v the volume fraction of impurity particles while *K* and *b* are constants. The pinning effects of oxide additives have been reported in numerous studies [102~104].

The weight changes of Cr_2O_3 with MgO additions after exposure to SCW environment at 650 ℃/25 MPa up to 600 hours are shown in Figure 4-15. MgO added Cr_2O_3 exhibited enhanced corrosion resistance with an increase of MgO content up to 5 wt. %. However when the addition amount increased to 8 wt. %, no improvement in corrosion resistance can be observed.

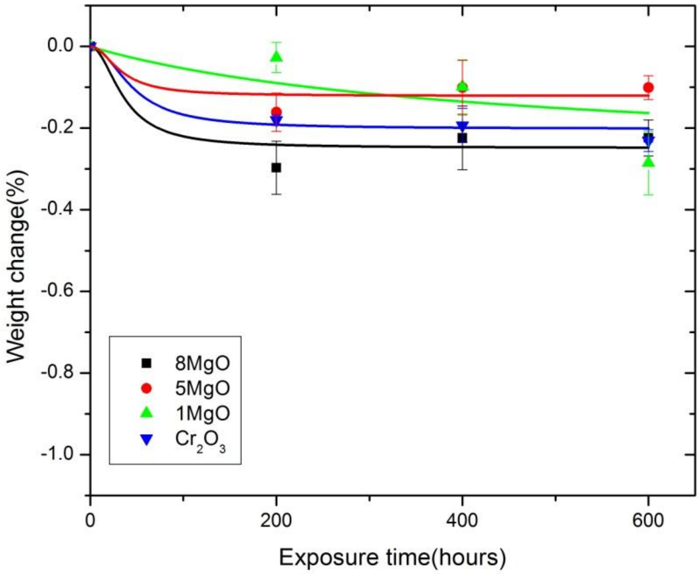

Figure 4-15. Weight changes of MgO added Cr_2O_3 ceramics exposed to SCW at 650 ℃/25 MPa for 200, 400 and 600 hours.

The results of mass spectrum analysis of the MgO added Cr_2O_3 after SCW exposure for 400 hours are presented in Figures 4-16 and 4-17. It can be seen that the concentration of soluble Cr-species was reduced when the addition content was below 5 wt. %. The beneficial effect of MgO can be originated from the formation of spinel phase. It was reported that $MgCr_2O_4$ was effective in blocking the migration of vacancies at the grain boundaries [105]. Consequently, the diffusion of O atoms along the grain boundaries can be restricted by the presence of spinel phase, which suppressed the oxidation of Cr^{3+}.

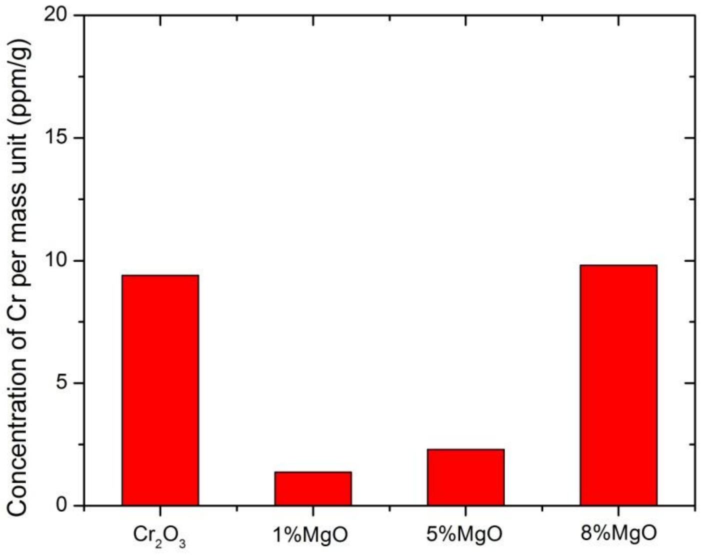

Figure 4-16. Concentrations of Cr in the water remained in the tube after MgO added Cr_2O_3 ceramics were exposed to SCW at 650 ℃/25 MPa for 400 hours. (The results were normalized by the weight of bulk ceramics.)

Nevertheless, it seemed that the concentration of dissolved Cr increased with higher addition of MgO and when the amount of MgO reached 8 wt. %, the concentration of dissolved Cr exceed that of pure Cr_2O_3. This increased dissolution at higher level of MgO addition could be caused by grain size refinement observed. As discussed in Section 4.1.3, the diffusion of oxygen at the grain boundaries is higher and materials with finer grain sizes have more grain boundary areas and would lead to more dissolution.

As can be observed from Figure 4-17, MgO itself can be instable in SCW with a dissolution rate of roughly 7 ppm per mass unit. However, owing to the role of diffusion barrier ($MgCr_2O_4$ spinel phase), very low rate of dissolution of Cr_2O_3 in terms of weight loss was observed when a low level of MgO was added. However, when the MgO content exceeded the critical value, the increased dissolution of Cr_2O_3 at can be triggered by the grain size refinement effects as discussed previously.

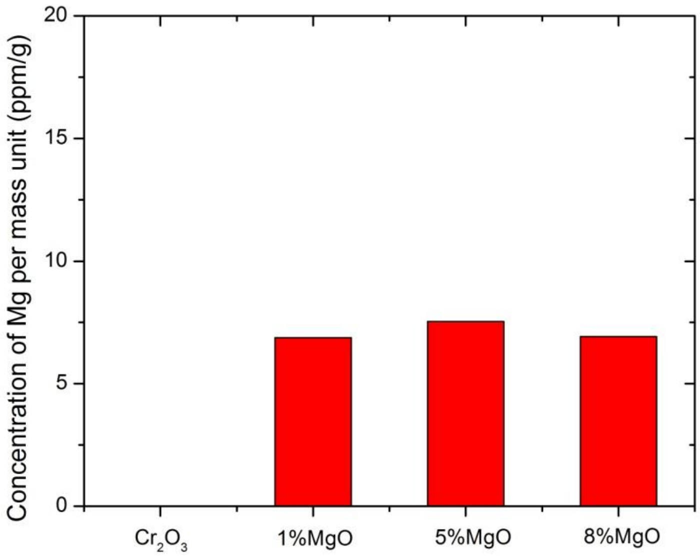

Figure 4-17. Concentrations of Mg in the water remained in the tube after MgO added Cr_2O_3 ceramics were exposed to SCW at 650 ℃/25 MPa for 400 hours. (The results were normalized by the weight of bulk ceramics.)

4.2.2 Effect of CeO_2 addition

The XRD results shown in Figure 4-18 indicated that for Cr_2O_3 ceramic added with 1 wt. % CeO_2, only the peaks belonging to Cr_2O_3 were identified. When the addition content increased to 5 wt. % or higher, the peaks corresponding to CeO_2 were also observed.

The SEM images of the as sintered CeO_2-added Cr_2O_3 are presented in Figure 4-19. It shows that the grain sizes of the ceramics were also influenced by the CeO_2 addition, probably through the grain boundary pinning effect. As shown in Table 4-4, similar to the MgO added Cr_2O_3, the average grain size of the CeO_2 added Cr_2O_3 also decreased when the addition content reached 8 wt. %, although the degree of refinement was not as significant as that seen in MgO added Cr_2O_3.

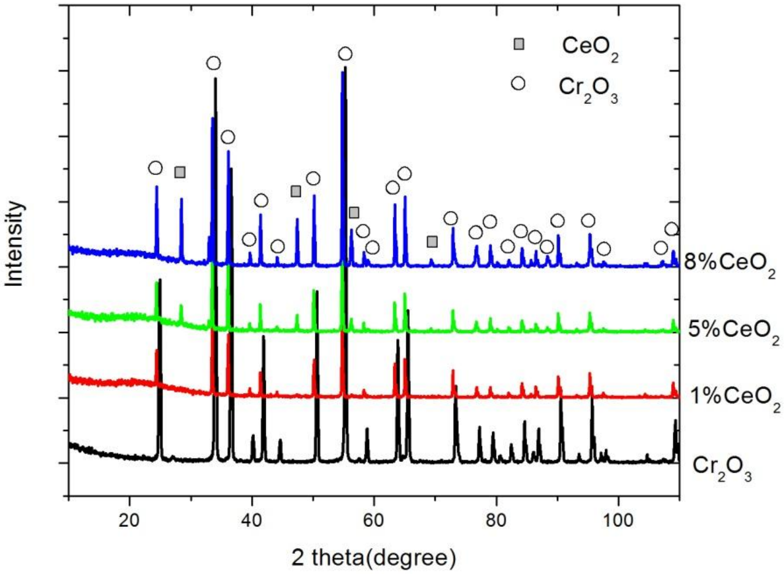

Figure 4-18. XRD patterns of CeO_2 added Cr_2O_3 ceramics compared with that of pure Cr_2O_3.

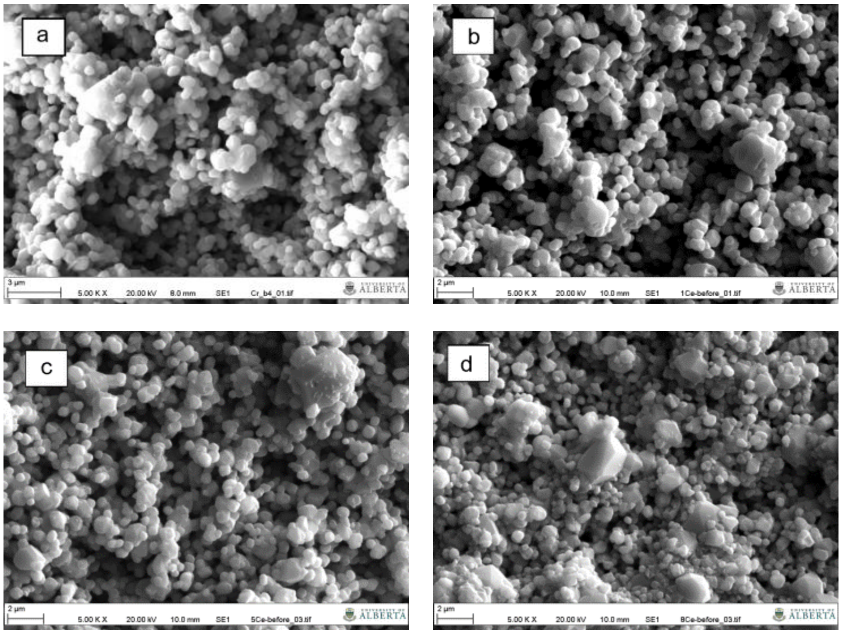

Figure 4-19. Surface morphologies of: (a) pure Cr_2O_3; (b) 1 wt. % CeO_2 added Cr_2O_3; (c) 5 wt. % CeO_2 added Cr_2O_3 and (d) 8 wt. % CeO_2 added Cr_2O_3.

Table 4-4. Estimated average grain sizes of Cr_2O_3 based ceramics with CeO_2 additions.

Sample	Average grain size(nm)
Cr_2O_3	453.5 ±14.4
Cr_2O_3+1 wt. % CeO_2	451.7 ±10.8
Cr_2O_3+5 wt. % CeO_2	452.5 ±12.2
Cr_2O_3+8 wt. % CeO_2	411.0 ±16.2

It can be seen from Figure 4-20 that when exposed to SCW at 650 ℃/ 25 MPa for up to 600 hours, weight changes of Cr_2O_3 based ceramics can be reduced by the addition of CeO_2, provided that the level of addition is below 5 wt. %. As the CeO_2 addition increased to 8 wt. %, large weight loss was observed.

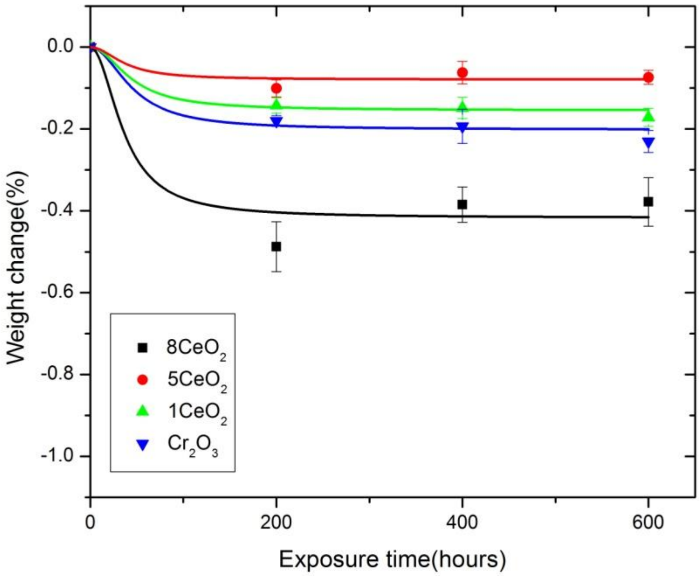

Figure 4-20. Weight changes of CeO_2 added Cr_2O_3 ceramics exposed to SCW at 650 ℃/25 MPa for 200, 400 and 600 hours.

The beneficial effect of CeO_2 can be attributed to the so-called “reactive element effects” [95]. When doped with CeO_2, due to their large atomic radius, Ce atoms tend to segregate at the grain boundaries where the distortion energy can be lowered. The segregation can impede the diffusion of O atoms, hence retarding the oxidation of Cr_2O_3. As a result, the dissolution rate of Cr was found to be reduced. The weight loss results were also consistent with the mass spectrum analysis of Cr shown in Figure 4-21, in which very low concentration of Cr-species was measured in the water remains after SCW exposure for specimens with a CeO_2 addition at or below 5 wt.%.

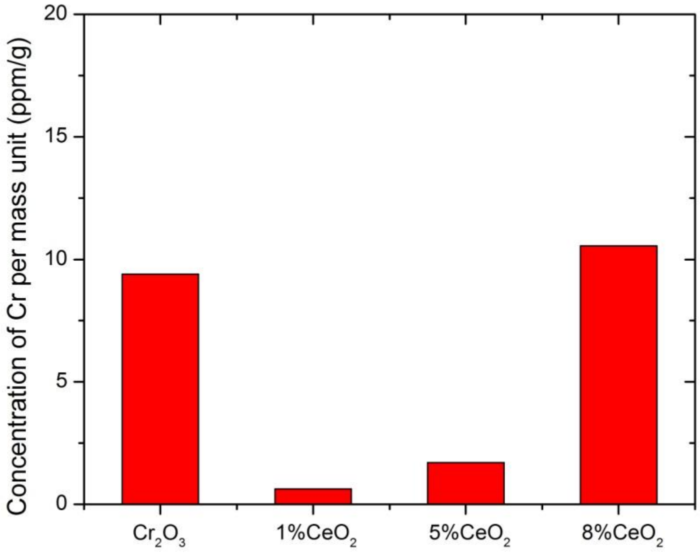

Figure 4-21. Concentrations of Cr in the water remained in the tube after CeO_2 added Cr_2O_3 ceramics were exposed to SCW at 650 ℃/25 MPa for 400 hours. (The results were normalized by the weight of bulk ceramics.)

Owing to the grain refinement effect, the dissolution of Cr was increased when CeO_2 content increased to 8 wt. %. According to Table 4-3 and Table 4-4, the Cr_2O_3 grains were less refined by CeO_2 addition as compared with the Cr_2O_3 ceramics with the same weight percentage of MgO addition. However, it was observed that the concentration of Cr in the water after the exposure of 8 wt. % CeO_2 added Cr_2O_3 was slightly higher, instead of lower, than that measured in the water remain after the exposure of 8 wt. % MgO added Cr_2O_3. This is because the amount of diffusion barrier $MgCr_2O_4$ formed increases with increasing MgO addition, which can somehow offset the effect of grain refinement; however since the solubility of CeO_2 in Cr_2O_3 was found to be quite limited (less than 3.5 wt. % at 1000 ℃ [106]), the fraction of CeO_2 solid solutions in Cr_2O_3 remained constant once the CeO_2 amounts exceeded its solubility, therefore the grain refinement can exert greater influence.

Figure 4-22 shows the concentration of Ce in the water after SCW test, which was found to be marginal (less than 0.2 ppm per mass unit). Thus it might be reasonable to conclude that under the current SCW conditions, the degradation of the CeO_2 added Cr_2O_3 ceramics was dominated by the dissolution of Cr_2O_3, which can be suppressed by the addition of CeO_2 through the reactive element effects but enhanced by the grain refinement effect when the CeO_2 content reached 8 wt. %.

Comparing the mass spectrum results of Mg (Figure 4-17) with those of Ce (Figure 4-22), it can be found that under the same SCW conditions, CeO_2 was much more stable than $MgCr_2O_4$ since the concentrations of Ce in the water were considerably lower. Therefore, Cr_2O_3 ceramics with proper amounts of CeO_2 additions were found to be more promising for SCWR applications.

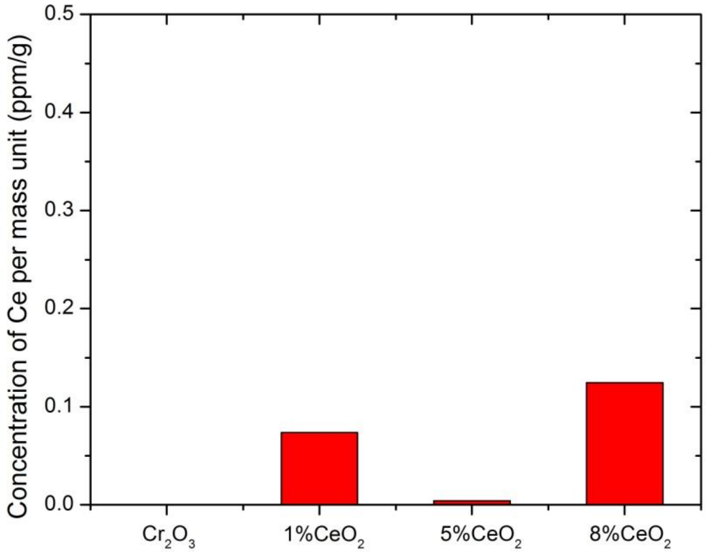

Figure 4-22. Concentrations of Cr in the water remained in the tube after CeO_2 added Cr_2O_3 ceramics were exposed to SCW at 650 ℃/25 MPa for 400 hours. (The results were normalized by the weight of bulk ceramics.)

4.2.3 Effect of SiO_2 addition

The phase diagram of SiO_2-Cr_2O_3 binary system is shown in Figure 4-23, which predict total immiscibility between SiO_2 and Cr_2O_3, as well as the absense of intermediate phases between Cr_2O_3 and SiO_2 under the sintering processes used in this investigation. This is consistent with the XRD results of the as sintered SiO_2 added Cr_2O_3 shown in Figure 4-24. The surface morphologies of the ceramics are shown in Figure 4-25.

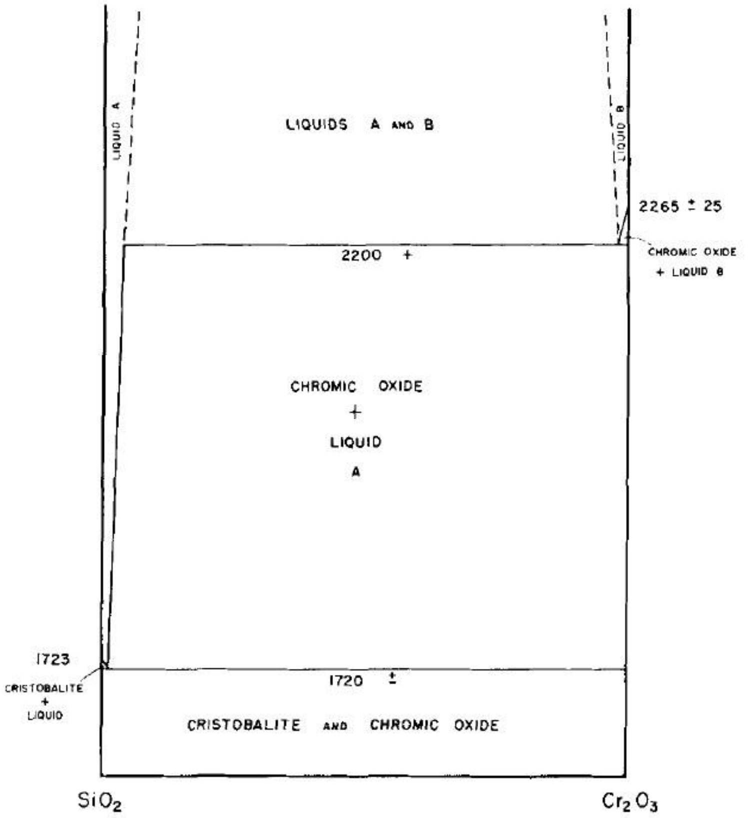

Figure 4-23. Phase diagram of Cr_2O_3-SiO_2 binary system [107].

Table 4-5 lists grain sizes of SiO_2 added Cr_2O_3 measured after sintering. Different from MgO or CeO_2 added Cr_2O_3, the grain refinement was seen to occur effectively at much lower level of SiO_2-addititon, roughly 1 wt. %.

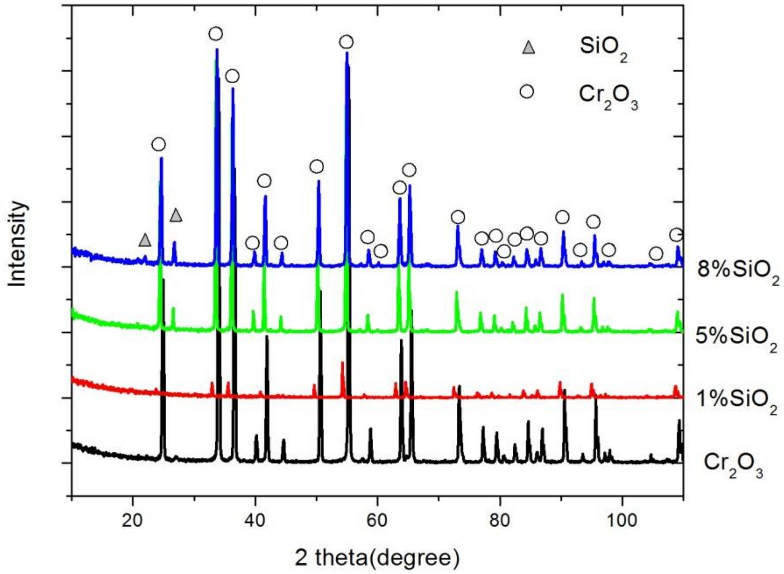

Figure 4-24. XRD patterns of SiO_2 added Cr_2O_3 ceramics compared with that of pure Cr_2O_3.

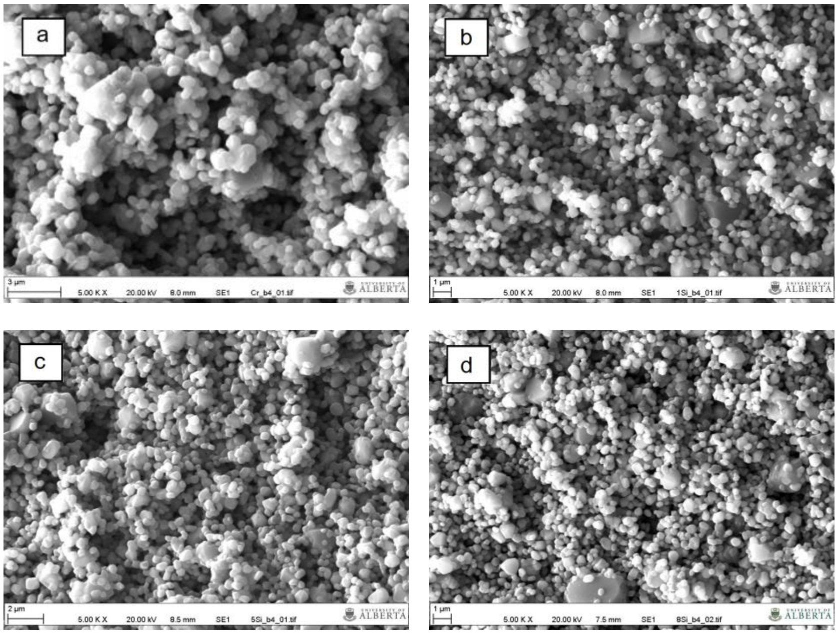

Figure 4-25. Surface morphologies of: (a) pure Cr_2O_3; (b) 1 wt. % SiO_2 added Cr_2O_3; (c) 5 wt. % SiO_2 added Cr_2O_3 and (d) 8 wt. % SiO_2 added Cr_2O_3.

Table 4-5. Estimated average grain sizes of Cr_2O_3 based ceramics with SiO_2 additions.

Sample	Average grain size(nm)
Cr_2O_3	453.5 ±14.4
Cr_2O_3+1 wt. % SiO_2	397.5 ±8.0
Cr_2O_3+5 wt. % SiO_2	377.0 ±13.3
Cr_2O_3+8 wt. % SiO_2	378.2 ±15.3

According to the test results shown in Figure 4-26, the Cr_2O_3 with all levels of SiO_2 addition has suffered severe attacks after exposure at 650 ℃/ 25 MPa for up to 600 hours in SCW, as compared with pure Cr_2O_3, indicating that SiO_2 addition was detrimental to the stability of Cr_2O_3 in SCW environment.

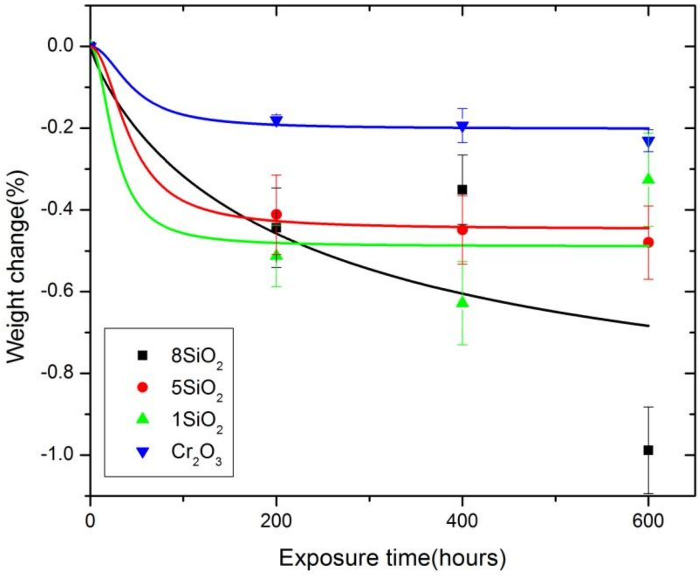

Figure 4-26. Weight changes of SiO_2 added Cr_2O_3 ceramics exposed to SCW at 650 ℃/25 MPa for 200, 400 and 600 hours.

Figures 4-27 and 4-28 show the concentrations of Cr and Si, respectively, in the water samples after SCW exposure for 400 hours as determined by mass spectrum analysis. The dissolution of Cr_2O_3 was found to be decreased for all SiO_2 added Cr_2O_3 samples, which seemed contradictory to the weight loss results shown in Fig. 4-26 and to the fact that SiO_2 added Cr_2O_3 had smaller grain size and would yield more dissolution of Cr_2O_3.

It was reported that Si may play a role as a reactive element like Ce [107]. This would suppress the dissolution of Cr_2O_3 and therefore a lower concentration of Cr-species in the water after SCW exposure can be expected for all SiO_2 added

Cr_2O_3, despite that finer grain size for the latter samples increases the dissolution of Cr_2O_3 as compared with pure Cr_2O_3.

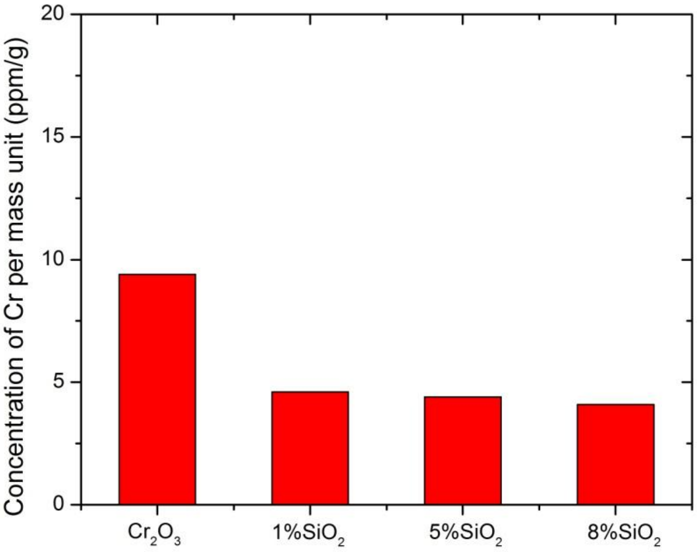

Figure 4-27. Concentrations of Cr in the water remained in the tube after SiO_2 added Cr_2O_3 ceramics were exposed to SCW at 650 ℃/25 MPa for 400 hours. (The results were normalized by the weight of bulk ceramics.)

Surprisingly, the concentration of Si-species remained in the water after SCW exposure was extremely high, which is around 80 times higher than that of Cr-species and 4000 times higher than that of Ce dissolved in the water after exposure. Therefore, the poor resistance of SiO_2 added Cr_2O_3 should be primarily attributed to the severe dissolution of SiO_2.

The solubility of SiO_2 in aqueous solution has been investigated in various studies. It has been reported that the hydration reaction occurred between SiO_2 and H_2O depends on the density of the solution [109]:

$$\mathrm{SiO_2 + 2H_2O \Leftrightarrow Si(OH)_4}, \text{ when density} \leq 0.05 \text{ g/ml;} \tag{10}$$

$$\mathrm{2SiO_2 + 3H_2O \Leftrightarrow Si_2O(OH)_6}, \text{ when } 0.1 \text{ g/ml} \leq \text{density} \leq 0.45 \text{ g/ml;} \tag{11}$$

$$\mathrm{SiO_2 + H_2O \Leftrightarrow SiO(OH)_2}, \text{ when density} \geq 0.65 \text{ g/ml} \tag{12}$$

As shown in Table 3-2, at the current SCW test conditions (650 ℃/25 MPa), the density of the water was proximately 0.0648 g/ml, corresponding to the transition zone where both reaction (10) and (11) may take place and a sharp increase in the dielectric constant can be achieved. The increase of dielectric constant is indicative of a higher polarity of the solution, which may lead to a higher solubility of SiO_2.

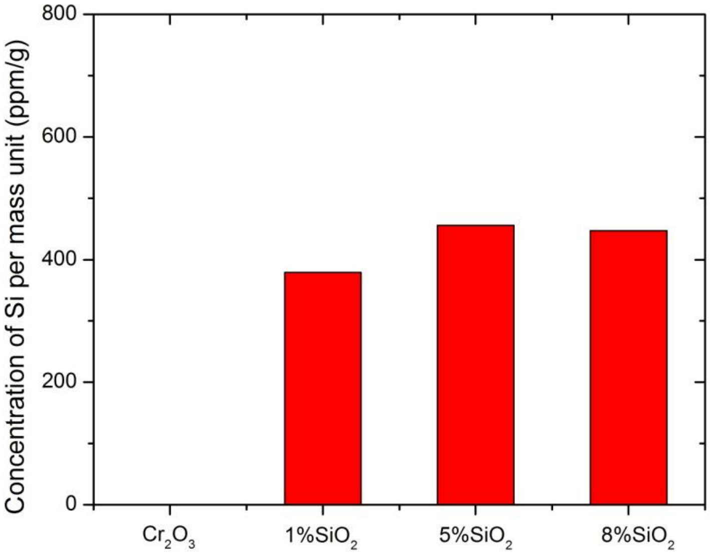

Figure 4-28. Concentrations of Si in the water remained in the tube after SiO_2 added Cr_2O_3 ceramics were exposed to SCW at 650 °C/25 MPa for 400 hours. (The results were normalized by the weight of bulk ceramics.)

To summarize, the result showed that introducing SiO_2 into Cr_2O_3 ceramics may cause severe degradation; hence SiO_2 addition should be cautiously avoided in the selection of SCWR candidate materials.

4.2.4 Effect of dissolved oxygen content on Cr_2O_3 with oxide additions

The corrosion responses of pure Cr_2O_3 ceramics to different levels of dissolved oxygen contents have been discussed in previous sections. It has been found that although higher oxygen content can promote the dissolution of Cr_2O_3, Cr_2O_3

ceramics exhibited weight gains due to the deposition of solid phases on the surface during cooling of the reactor.

The stabilities of Cr_2O_3 with other oxide additions in SCW with higher oxygen content were also examined. The SCW test conditions were kept identical with those described in Sections 4.2.1~4.2.3 except for the oxygen content. In the current study, 30% H_2O_2, rather than deionized water, was added into the capsules, which raised the oxygen content from 3920 ppm for the case of using deionized water to 168925 ppm for the 30% H_2O_2. The obtained results in terms of weight changes after SCW exposure are presented in Figures 4-29 through 4-31. The mass spectrum tests results of the ceramics after exposure for 400 hours are shown in Figures 4-32 through 4-34.

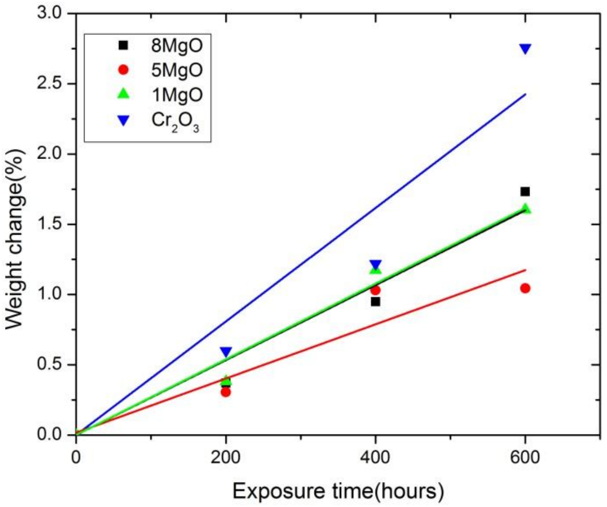

Figure 4-29. Weight changes of MgO added Cr_2O_3 ceramics exposed to SCW with 30% H_2O_2 at 650 ℃/25 MPa for 200, 400 and 600 hours.

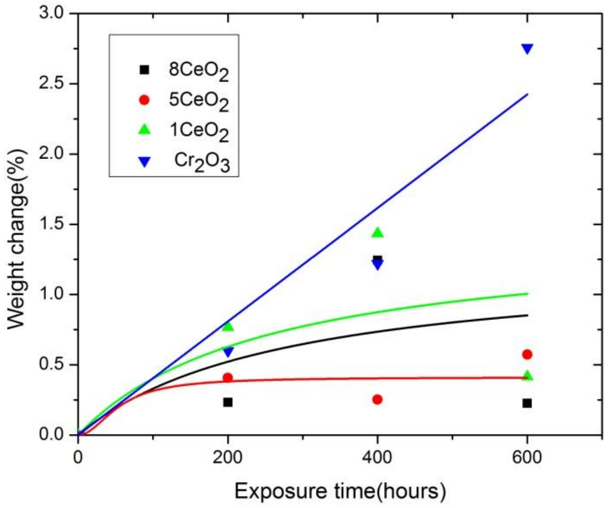

Figure 4-30. Weight changes of CeO_2 added Cr_2O_3 ceramics exposed to SCW with 30% H_2O_2 at 650 ℃/25 MPa for 200, 400 and 600 hours.

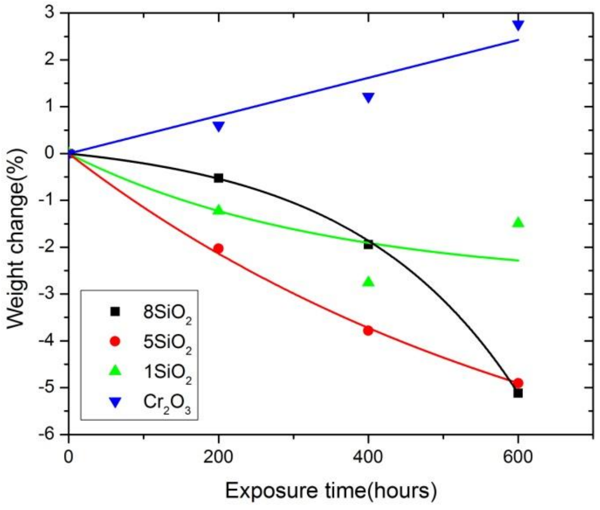

Figure 4-31. Weight changes of SiO_2 added Cr_2O_3 ceramics exposed to SCW with 30% H_2O_2 at 650 ℃/25 MPa for 200, 400 and 600 hours.

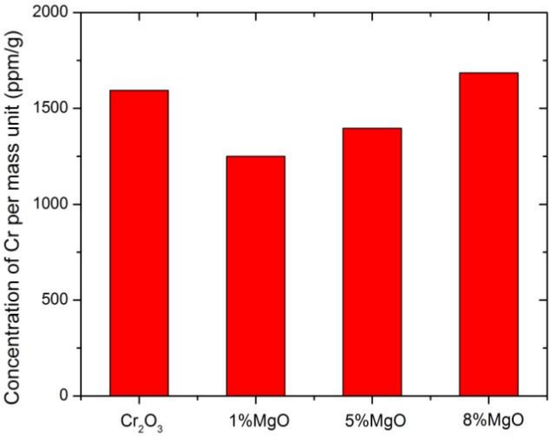

(a)

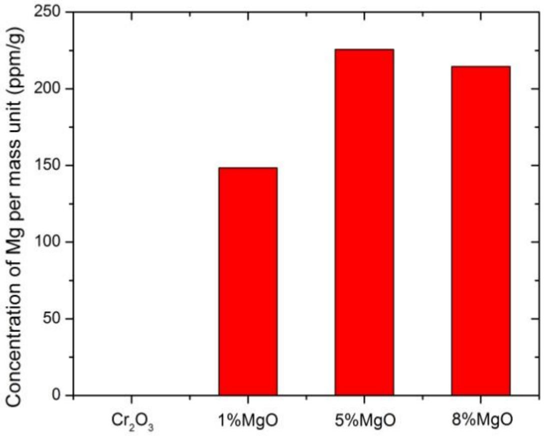

(b)

Figure 4-32. Concentrations of: (a) Cr; (b) Mg in the water remained in the tube after MgO added Cr_2O_3 ceramics were exposed to SCW with 30% H_2O_2 at 650 ℃/25 MPa for 400 hours. (The results were normalized by the weight of bulk ceramics.)

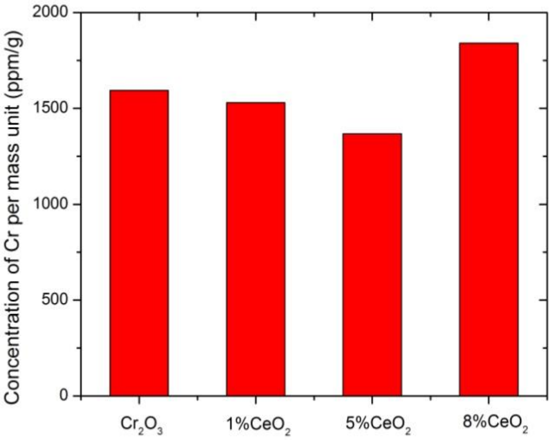

(a)

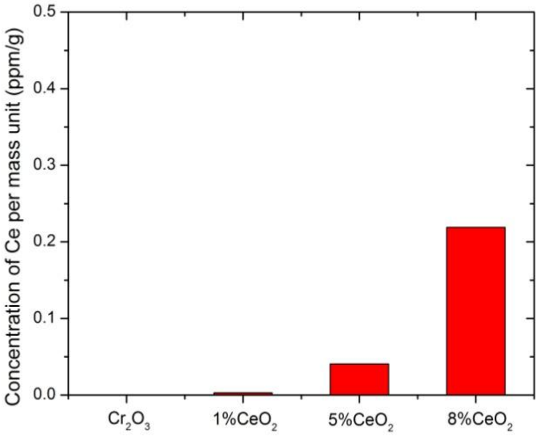

(b)

Figure 4-33. Concentrations of: (a) Cr; (b) Ce in the water remained in the tube after CeO_2 added Cr_2O_3 ceramics were exposed to SCW with 30% H_2O_2 at 650 ℃/25 MPa for 400 hours. (The results were normalized by the weight of bulk ceramics.)

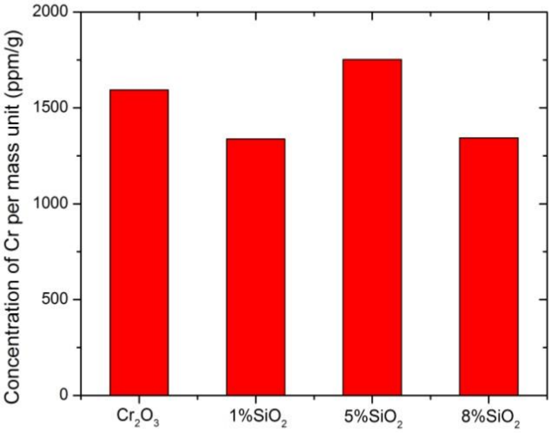

(a)

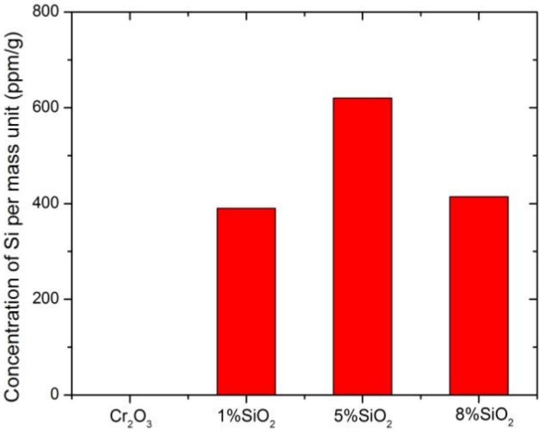

(b)

Figure 4-34. Concentrations of: (a) Cr; (b) Si in the water remained in the tube after SiO_2 added Cr_2O_3 ceramics were exposed to SCW with 30% H_2O_2 at 650 ℃/25 MPa for 400 hours. (The results were normalized by the weight of bulk ceramics.)

It can be seen that the all MgO and CeO_2 added Cr_2O_3 ceramics showed weight gains, whereas SiO_2 added Cr_2O_3 exhibited large weight losses. Similar to pure Cr_2O_3, depositions of large particles enriched in Ca and Mo can also be observed on the surface of additives added Cr_2O_3 after SCW tests, which should be responsible for the increased weight gains despite that severe dissolution of Cr_2O_3 had occurred. Examples of particles deposited on the ceramics surface are shown in Figure 4-35.

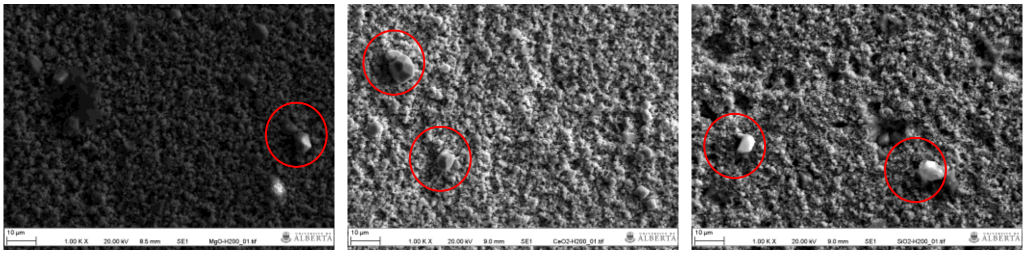

(a) (b) (c)

Figure 4-35. Surface morphologies of: (a) 8 wt. % MgO added Cr_2O_3; (b) 8 wt. % CeO_2 added Cr_2O_3 and (c) 8 wt. % SiO_2 added Cr_2O_3 after Cr_2O_3 based ceramics were exposed to SCW with 30% H_2O_2 at 650 ℃/25 MPa for 200 hours. (The large depositions observed on the ceramic surface were marked by circles.)

According to Figures 4-29 and 4-30, the weigh gains of MgO and CeO_2 added Cr_2O_3 were found to be smaller than those of pure Cr_2O_3. This observation can be explained by the outward diffusion of Ca in the ceramics. In order to react with Mo^{6+} in the liquid and to subsequently form $CaMoO_4$ deposition on the ceramic surface, Ca atoms inside the ceramics need to constantly diffuse outward to the surface via short circuit paths (grain boundaries). According to the aforementioned discussions, the formation of $MgCr_2O_4$ or the solid solution between Ce and Cr_2O_3 can act as diffusion barriers at the grain boundaries. Therefore, the reduced weigh gain may be attributed to those diffusion barriers which hindered the outward diffusion of Ca and obstructed the formation of Ca and Mo enriched depositions. Similar to the inward diffusion of O, the suppression effects induced by MgO or CeO_2 additives on Ca outward diffusion became stronger as the addition content reached 5 wt. %, at which the least weigh gain was observed. The weight gains increased as the addition content increased to 8 wt. %, which may also result from the grain refinement. It is worth mentioning that the dissolution rate of MgO, as shown in Figure 4-32 b, was found to be tremendous, which may also partially contribute to the decreased weight gains for Cr_2O_3 with MgO additions. The weight loss observed for SiO_2 added Cr_2O_3 was most likely because of the high dissolution rate of SiO_2, which prevailed the weight gains caused by the deposition of new oxide phases as identified.

The concentrations of Cr-species dissolved in the water (Figures 4-32 a, 4-33 a and 4-34 a) showed similar trends with those of oxide added ceramics exposed in low oxygen-containing SCW. It was found that in SCW with high dissolved oxygen content, the dissolution of Cr_2O_3 can also be suppressed by the introduction of $MgCr_2O_4$ or reactive elements and be promoted by the grain refinement of the ceramics. Nevertheless, it seemed that those effects induced by the additives, either beneficial or detrimental on the Cr dissolution, were not as significant as those in low oxygen containing SCW. This implied that as the oxygen content increased, the diffusion of oxygen became less dependent on the diffusion paths, and the effects of oxide additives on the stability of Cr_2O_3 based ceramics were thereafter weakened.

Comparing Figure 4-32 b with Figure 4-17 revealed that the stability of MgO in SCW was highly dependent on the dissolved oxygen content, and in SCW with high oxygen levels the dissolution rate of MgO can be 20~30 times greater. However, the stabilities of CeO_2 and SiO_2 seemed to be hardly affected by the dissolved oxygen content.

4.2.5 Summary

The effects of MgO, CeO_2, and SiO_2 additions on the stabilities of Cr_2O_3 based ceramics in SCW environments with two levels of dissolved oxygen were investigated in this section. The results showed that 1 wt. % and 5 wt. % MgO and CeO_2 additives can reduce the dissolution of Cr_2O_3. The successful blockage of the oxygen diffusion induced by $MgCr_2O_4$ or reactive element Ce might be accountable for the improved stability. However, as the dissolved oxygen content increased, the beneficial effect of MgO and CeO_2 became less significant. The pinning effect brought by the introduction of secondary oxide particles resulted in grain refinement, which led to the higher dissolution rate of Cr_2O_3 when the addition content exceeded the critical value. Adding SiO_2 can decrease the stability of Cr_2O_3 based ceramics dramatically because of its high solubility in SCW. Among the three oxide additives, CeO_2 added Cr_2O_3 exhibited the best resistance to dissolution in SCW whereas SiO_2 added Cr_2O_3 the lowest. The stability of MgO was found to be intermediate, but it can be affected strongly by the dissolved oxygen content.

Chapter 5 Summary and suggested future work

In this study, the effects of dissolved oxygen content, grain size as well as various oxide additives on the stabilities of Cr_2O_3 based ceramics in supercritical water environment were examined. The following conclusions have been drawn:

1. Cr_2O_3 ceramic can be unstable in SCW at 650 ℃/25 MPa, and it can react with water and oxygen to form soluble H_2CrO_4 species.

2. The stability of Cr_2O_3 in SCW was closely related to its grain size. As the grain size decreased, more oxygen diffusion paths were created, which led to greater oxidation rate.

3. By adding certain amounts of MgO, CeO_2 or SiO_2, the grain size of Cr_2O_3 based ceramic was reduced evidently, which can be attributed to the pinning effect induced by the secondary particles during the sintering process.

4. It was found that adding proper amounts (≤ 5 wt. %) of MgO and CeO_2 can enhance the stabilities of Cr_2O_3 based ceramics, which may be attributed to the presence of diffusion barriers ($MgCr_2O_4$ or reactive element Ce). When the addition content increased to 8 wt. %, the higher

oxygen diffusion rate, resulting from the grain refinement induced by the oxide additives, can accelerate the degradation of Cr_2O_3 based ceramics. The addition of SiO_2 was detrimental to the stability of Cr_2O_3 in the SCW environment owing to the great solubility of Si in SCW environment.

5. Dissolved oxygen content can exert great influence on the stability of Cr_2O_3 in SCW environment; the concentration of Cr in the water increased tremendously when the dissolved oxygen content was elevated from 3920 ppm to 168925 ppm. However, weight gain instead of weight loss was observed after Cr_2O_3 ceramic was exposed to SCW with high dissolved oxygen content, which may result from the deposition of Ca and Mo enriched species on the ceramic surface. As dissolved oxygen content increased, the beneficial effects of the oxide additions on inhibiting the dissolution of Cr became less significant.

6. Of all the additives examined in the current study, CeO_2 added Cr_2O_3 showed the best stability in SCW, followed by MgO and SiO_2 added Cr_2O_3. The dissolution rate of MgO added Cr_2O_3 in SCW increased remarkably as the dissolved oxygen content built up, whereas the influence of the content of oxygen on the stabilities of CeO_2 and SiO_2 added Cr_2O_3 was found to be marginal.
7. The current study indicated that pure Cr_2O_3 is not recommending as structure or coating materials in SCWR since it can be dissolved,

especially when the oxygen content of the SCW is high. However, proper modifications (introducing CeO_2 additions or increasing the grain size) of the Cr_2O_3 ceramics can improve its stability and increase the feasibility of applying Cr_2O_3 in SCW environment. Other measures can also be taken to improve the properties of those Cr_2O_3 based ceramics in order to better fulfill the operating requirement in SCWR. (For instance, increasing the porosity so a better thermal insulation can be offered.)

Future efforts in the following perspectives are highly recommended:

1. The effects of various fabrication methods on the stability of Cr_2O_3 based ceramics in SCW.

   It is commonly acknowledged that the properties of ceramics are highly dependent on the processing methods and parameters used. However, in the current study the sintering parameters of the ceramics was fixed (1200 ℃ for 15 hours in air), and the obtained ceramics were found to be quite porous. Therefore in the future, it might be of great interest to adjust the sintering parameters or to prepare ceramics using other methods.

2. The stabilities of Cr_2O_3 based ceramics in SCW with different temperatures and pH values.

   The SCW tests in the current study were all conducted at 650 ℃ and 25 MPa. Nevertheless, since the operating temperautres of different components in SCWR may vary from 350 ℃ to 850 ℃, the effect of temperaures must be are in need in order to provide a more comprehensive understanding of the fesibility of applying Cr_2O_3 based materials in SCWR,. pH is another crucial parameter that can affect the stabilities of Cr_2O_3 based ceramics significantly, thus SCW test in acidic or alkline environment may also be considered.

3. The improvement of the SCW test configurations.

   The static reactors adopted in the current study showed it inferiority when conducted SCW test in high dissolved oxygen content. Large depositions were found on the ceramics surfaces, which may mask the authentic stabilities of the ceramics. This problem might be improved by conducting tests in an SCW loop, where the water can be constantly renewed to wash away the corrosion products.

Bibliography:

[1] G.S. Was, S. Teysseyre, “Challenges and recent progress in corrosion and stress corrosion cracking of alloys for supercritical water reactor core components”, Proceeding of the 12th International Conference on Environmental Degradation of Materials in Nuclear Power System, Salt Lake City, Utah, USA, 2005, August 14-18.

[2] P.E. Savage, “Organic chemical reactions in supercritical water”, Chem. Rev., Vol. 99, 1999, pp. 603-621.

[3] Y. Oka and S. Koshizuka, “Supercritical-pressure, once-through cycle light water cooled reactor concept”, Journal of Nuclear Science and Technology, Vol. 38, No. 12, 2001, pp. 1081-1089.

[4] D. Squarer, T. Schulenberg, D. Struwe, Y. Oka, D. Bittermann, N. Aksan, C. Maraczy, R. Kyrki-Rajamäki, A. Souyri and P. Dumaz, “High performance light water reactor”, Nuclear Engineering and Design, Vol. 221, 2003, pp. 167-180.

[5] H. Khartabil, “SCWR: overview”, GIF Symposium, Paris, France, 2009, September 9-10.

[6] T. Reiss, Gy. Csom, S. Feher and Sz. Czifrus, “The Simplified Supercritical Water-Cooled Reactor (SSCWR), a new SCWR design”, Progress in Nuclear Energy, Vol. 52, 2010, pp. 177-189.

[7] X. Cheng, T. Schulenberg, D. Bittermann and P. Rau, “Design analysis of core assemblies for supercritical pressure conditions”, Nuclear Engineering and Design, Vol. 223, 2003, pp. 279-294.

[8] Y. Bae, J. Jang, H. Kim, H. Yoon, H. Kang and K. Bae, “Research activities on a supercritical pressure water reactor in Korea”, Nuclear Engineering and Technology, Vol. 39, No. 4, 2007, pp. 273-286.

[9] J. Shan, B. Zhang, C. Li and L.K.H. Leung, “SCWR subchannel code ATHAS development and CANDU-SCWR analysis”, Nuclear Engineering and Design, Vol. 239, 2009, pp. 1979-1987.

[10] R.B. Duffey, I.L. Pioro, B.A. Gabaraev and Yu.N. Kuznetsov, “SCW pressure-channel nuclear reactors: some design features and concepts”, Proceedings of ICONE14 International Conference on Nuclear Engineering, Miami, Florida, USA, 2006, July 17-20.

[11] C.K. Chow and H.F. Khartabil, “Conceptual fuel channel designs for Candu-SCWR”, Nuclear Engineering and Technology, Vol. 40, No. 2, 2007, pp. 139-146.

[12] J. Samuel, “Conceptual design for a re-entrant type fuel channel for supercritical water-cooled nuclear reactors”, Unpublished master's thesis, University of Ontario Institute of Technology, Ottawa, Canada.

[13] F. Zarandi and W.R. Tyson, “Challenges in mechanical performance of materials in SCWR”, The 2nd Canada-China Joint Workshop on Supercritical Water-Cooled Reactors, Toronto, Canada, 2010, April 25-28.

[14] R.L. Klueh and A.T. Nelson, “Ferritic/martensitic steels for next-generation reactors”, Journal of Nuclear Materials, Vol. 371, 2007, pp. 37-52.

[15] S.S. Hwang, B.H. Lee, J.G. Kim and J. Jang, “SCC and corrosion evaluations of the F/M steels for a supercritical water reactor”, Journal of Nuclear Materials, Vol. 372, 2008, pp. 177-182.

[16] P. Ampornrat and G.S. Was, “Oxidation of ferritic-martensitic alloys T91, HCM12A and HT-9 in supercritical water”, Journal of Nuclear Materials, Vol. 371, 2007, pp. 1-17.

[17] K. Yin, S. Qiu, R. Tang, Q. Zhang and L. Zhang, “Corrosion behavior of ferritic/martensitic steel P92 in supercritical water”, The Journal of Supercritical Fluids, Vol. 50, 2009, pp. 235-239.

[18] Y. Chen, K. Sridharan and T. Allen, “Corrosion behavior of ferritic-martensitic steel T91 in supercritical water”, Corrosion Science, Vol. 48, 2006, pp. 2843-2854.

[19] X. Ren, K. Sridharan and T.R. Allen, “Corrosion of ferritic-martensitic steel HT9 in supercritical water”, Journal of Nuclear Materials, Vol. 358, 2006, pp. 227-234.

[20] L. Tan, X. Ren and T.R. Allen, “Corrosion behavior of 9-12% Cr ferritic-martensitic steels in supercritical water”, Corrosion Science, Vol. 52, 2010, pp. 1520-1528.

[21] Y. Chen, K. Sridharan, S. Ukai and T.R. Allen, “Oxidation of 9Cr oxide dispersion strengthened steel exposed in supercritical water”, Journal of Nuclear Materials, Vol. 371, 2007, pp. 118-128.

[22] L. Tan, Y. Yang and T.R. Allen, “Oxidation behavior of iron-based alloy HCM12A exposed in supercritical water”, Corrosion Science, Vol. 48, 2006, pp. 3123-3128.

[23] Z. Zhou, M. Li, L. Liao, X. Liu, P. He, Y. Xu, W. Chen and C. Ge, “The recent development of fabrication of ODS ferritic steels for supercritical water-

cooled reactors core application", The 2nd Canada-China Joint Workshop on Supercritical Water-Cooled Reactors, Toronto, Canada, 2010, April 25-28.

[24] M. Li, Z. Zhou, L. Liao, W. Chen and C. Ge, "High temperature oxidation behavior of ODS iron-base alloys for nuclear energy application", The 2nd Canada-China Joint Workshop on Supercritical Water-Cooled Reactors, Toronto, Canada, 2010, April 25-28.

[25] H.S. Cho, A. Kimura, S. Ukai and M. Fujiwara, "Corrosion properties of oxide dispersion strengthened steels in super-critical water environment", Journal of Nuclear Materials, Vol. 329-333, 2004, pp. 387-391.

[26] Y. Chen, K. Sridharan and T.R. Allen, "Corrosion behavior of NF616 and D9 as candidate alloys for supercritical water reactors", NACE Corrosion Conference 2005, Houston, USA, 2005, April 3-7.

[27] X. Luo, R. Tang, C. Long, Z. Miao, Q. Peng and C. Li, "Corrosion behavior of austenitic and ferritic steels in supercritical water", Nuclear Engineering and Technology, Vol. 40, No. 2, 2007, pp. 147-154.

[28] G.S. Was, S. Teysseyre and Z. Jiao, "Corrosion of austenitic alloys in supercritical water", Corrosion, Vol. 62, No. 11, 2006, pp. 989-1005.

[29] Y. Chen, K. Sridharan and T.R. Allen, "Corrosion of candidate austenitic stainless steels for supercritical water reactors", NACE Corrosion Conference 2007, Nashville, USA, 2007, March 11-15.

[30] G. S. Was, S. Teysseyre and J. McKinley, "Corrosion and stress corrosion cracking of iron- and nickel-base austenitic alloys in supercritical water", NACE Corrosion Conference 2004, New Orleans, USA, 2004, March 28-April 1.

[31] N. Zhang, Y. Bai, X. Yuan, B. Li and H. Xu, “Corrosion behavior of austenitic and ferritic/martensitic steels exposed in supercritical water with dissolved oxygen”, Applied Mechanics and Materials, Vol. 71-78, 2001, pp. 2916-2919.

[32] M. Da Cunha Belo, M. Walls, N.E. Hakiki, J. Corset, E. Picquenard, G. Sagon and D. Noel, “Composition, structure and properties of the oxide films formed on the stainless steel 316L in a primary type PWR environment”, Corrosion Science, Vol. 40, No. 2/3, 1998, pp. 447-463.

[33] S.H. Nie, Y. Chen, X. Ren, K. Sridharan and T.R. Allen, “Corrosion of alumina-forming austenitic steel Fe-20Ni-14Cr-3Al-0.6Nb-0.1Ti in supercritical water”, Journal of Nuclear Materials, Vol. 339, 2010, pp. 231-235.

[34] J. Mckinley, S. Teysseyre, and G. S. Was, D. B. Mitton, H. Kim, J-K Kim and R. M. Latanision, “Corrosion and stress corrosion cracking of austenitic alloys in supercritical water”, GENES4/ANP2003, Kyoto, Japan, 2003, September 15-19.

[35] N. Zhang, B. Li, Y. Bai and H. Xu, “Oxidation of austenitic steel TP347HFG exposed to supercritical water with different dissolved oxygen concentration”, Applied Mechanics and Materials, Vol. 148-149, 2012, pp. 1179-1183.

[36] Y. Nakazono, T. Iwai and H. Abe, “General corrosion properties of modified PNC1520 austenitic stainless steel in supercritical water as a fuel cladding candidate material for supercritical water reactor”, Joint AIRAPT-22 & HPCJ-50, Odaiba, Japan, 2009, July 26-31.

[37] T.R. Allen, “Novel techniques to mitigate corrosion and stress corrosion cracking in supercritical water”, NACE Corrosion Conference 2007, Nashville, USA, 2007, March 11-15.

[38] K. Sridharan, Y. Chen, L. Tan, X. Ren, A. Kruizenga, M. Anderson, and T. Allen, “Perspectives on corrosion in supercritical water environment: materials and novel treatments”, NACE Corrosion Conference 2009, Atlanta, USA, 2009, March 22-29.

[39] L. Zhang, Y. Bao and R. Tang, “Selection and corrosion evaluation tests of candidate SCWR fuel cladding materials”, Nuclear Engineering and Design, Vol. 249, 2012, pp. 180-187.

[40] Y. Tsuchiya, F. Kano, N. Saito, and M. Ookawa, “Corrosion and SCC properties of fine grain stainless steel in subcritical and supercritical pure water”, NACE Corrosion Conference 2007, Nashville, USA, 2007, March 11-15.

[41] Y. Ma and D.G. Lu, “High-temperature stress rupture performance of hastelloy C-27”, The 2nd Canada-China Joint Workshop on Supercritical Water-Cooled Reactors, Toronto, Canada, 2010, April 25-28.

[42] L. Tan, X. Ren, K. Sridharan and T.R. Allen, “Corrosion behavior of Ni-base alloys for advanced high temperature water-cooled nuclear plants”, Corrosion Science, Vol. 50, 2008, pp. 3052-3056.

[43] Y. Daigo, Y. Watanabe, K. Sugahara and T. Isobe, “Compatibility of nickel-based alloys with supercritical water applications: aging effects on corrosion resistance and mechanical properties”, Corrosion, Vol. 62, No. 2, 2006, pp. 174-181.

[44] Z.Y. Chen, J.L. Luo, W.X. Chen, W. Zheng and D.A. Guzonas, “Stress corrosion cracking of 316 ss and alloy 625 in supercritical water”, The 2nd Canada-China Joint Workshop on Supercritical Water-Cooled Reactors, Toronto, Canada, 2010, April 25-28.

[45] R. Fujisawa, K. Nishimura, T. Nishida, M. Sakaihara, Y. Kurata and Y. Watanabe, “Corrosion behavior of nickel-based alloys and type 316 stainless steel in slightly oxidizing or reducing supercritical water”, Corrosion, Vol. 62, No. 3, 2006, pp. 270-274.

[46] Q. Zhang, R. Tang, C. Li, X. Luo, C. Long and K. Yin, “Corrosion behavior of Ni-base alloys in supercritical water”, Nuclear Engineering and Technology, Vol. 41, No. 1, 2009, pp. 107-112.

[47] K. Sugahara and T. Isobe, “Improved compatibility of a new Ni base alloy with supercritical water applications: beneficial effects of Ta addition on corrosion resistance and aging susceptibility”, NACE Corrosion Conference 2004, New Orleans, USA, 2004, March 28-April 1.

[48] Q. Peng, E. Gartner, J.T. Busby, A.T. Motta, and G.S. Was, “Corrosion behavior of model zirconium alloys in deaerated supercritical water at 500°C”, Corrosion, Vol. 63, No. 3, 2007, pp. 577-590.

[49] A.T. Motta, A. Yilmazbayhan, M.J. Gomes da Silva, R.J. Comstock, G.S. Was, J.T. Busby, E. Gartner, Q. Peng, Y.H. Jeong, J.Y. Park, “Zirconium alloys for supercritical water reactor applications: Challenges and possibilities”, Journal of Nuclear Materials, Vol. 371, 2007, pp. 61-75.

[50] Y.H. Jeong, J.Y. Park, H.G. Kim, J. T. Busby, E. Gartner, M. Atzmon, G. S. Was, R.J. Comstock, Y.S. Chu, M. Gomes da Silva, A. Yilmazbayhan and A.T. Motta, “Corrosion of zirconium-based fuel cladding alloys in supercritical water”, Proceeding of the 12th International Conference on Environmental Degradation of Materials in Nuclear Power System, Salt Lake City, USA, 2005, August 14-18.

[51] J. Wang, H. Fan, J. Xiong, H. Liu, Z. Miao, S. Ying, G. Yang, “Effects of Fe and Cr on corrosion behavior of ZrFeCr alloys in 500℃ steam”, Nuclear Engineering and Design, Vol. 241, 2011, pp. 471-475.

[52] S. Kasahara, J. Kuniya, K. Moriya, N. Saito and S. Shiga, “General corrosion of iron, nickel and titanium alloys as candidate materials for the fuel claddings of the supercritical-water cooled power reactor”, GENES4/ANP2003, Kyoto, Japan, 2003, September 15-19.

[53] J. Kaneda, S. Kasahara, J. Kuniya, K. Moriya, F. Kano, N. Saito, A. Shioiri, T. Shibayama and H. Takahashi, “General corrosion properties of titanium based alloys for the fuel claddings in the supercritical water-cooled reactor”, Proceeding of the 12th International Conference on Environmental Degradation of Materials in Nuclear Power System, Salt Lake City, USA, 2005, August 14-18.

[54] N. Boukis, N. Claussen, K. Ebert, R. Janssen and M. Schacht, “Corrosion screening tests of high-performance ceramics in supercritical water containing oxygen and hydrochloric acid”, Journal of the Europeun Ceramic Society, Vol. 17, 1997, pp. 71-76.

[55] H. Li, K. Liang, L. Mei, S. Gu, S. Wang, “Oxidation protection of mild steel by zirconia sol–gel coatings”, Materials Letters, Vol. 51, 2001, pp. 320-324.

[56] S. Block, J.A.H. Da Jornada, and G.J. Piermarini, “Pressure-temperature phase diagram of zirconia”, J. Am. Ceram. Soc, Vol. 68, No. 9, 1985, pp. 497-499.

[57] M.A. Domínguez-Crespoa, A. García-Murillo, A.M. Torres-Huerta, F.J. Carrillo-Romo, E. Onofre-Bustamante, C. Yanez-Zamora, “Characterization of ceramic sol-gel coatings as an alternative chemical conversion treatment on commercial carbon steel”, Electrochimica Acta, Vol. 54, 2009, pp. 2932-2940.

[58] R.L. Jones, “Some aspects of the hot corrosion of thermal barrier coatings”, Journal of Thermal Spray Technology, Vol. 6, No. 1, 1997, pp. 77-84.

[59] G.T. Hong, W.R. Killilea, D.W. Ordway, “Zirconium oxide ceramics for surfaces exposed to high temperature water oxidation environments”, U.S. Patent 5,358,645, issued Oct. 25, 1994.

[60] D.A. Guzonas, J.S. Wills, G.A. McRae, S. Sullivan, K. Chu, K. Heaslip and M. Stone, “Corrosion-resistant coatings for use in a supercritical water CANDU reactor”, Proceeding of the 12th International Conference on Environmental Degradation of Materials in Nuclear Power System, Salt Lake City, USA, 2005, August 14-18.

[61] A.R. Shankar, U. K. Mudali, R. Sole, H.S. Khatak, B. Raj, “Plasma-sprayed yttria-stabilized zirconia coatings on type 316L stainless steel for pyrochemical reprocessing plant”, Journal of Nuclear Materials, Vol. 372, 2008, pp. 226-232.

[62] F.P. Orfino, B. Yao, Y. Xie, S. Yick, J. Miles, W. Cook and R. Hui, “Ceramic coatings for metallic components in supercritical water cooled reactors”, The 5th Int. Sym. SCWR, Vancouver, Canada, 2011, March 13-16.

[63] M. R. Howlader, K. Shiiyama and C. Kinoshita, “The electrical conductivity of zircaloy oxide films”, Journal of Nuclear Materials, Vol. 253, No. 1-3, 1998, pp. 149-155.

[64] X. Nie, E.I. Meletis, J.C. Jiang, A. Leyland, A.L. Yerokhin and A. Matthews, “Abrasive wear/corrosion properties and TEM analysis of Al_2O_3 coatings fabricated using plasma electrolysis”, Surface and Coatings Technology, Vol. 149, 2002, pp. 245-251.

[65] B. Liu, B.Y. Jiang, Y. Fu, D.J. Cheng, X.F. Wu, S.Z. Yang, “Alumina, aluminium nitride and aluminium composite coating on 0.45% C steel by using a plasma source ion implantation and deposition (PSII&D) system”, Thin Solid Films, Vol. 349, 1999, pp.110-114.

[66] M. Schacht, N. Boukis, E. Dinjus, “Corrosion of alumina ceramics in acidic aqueous solutions at high temperatures and pressures”, Journal of Materials Science, Vol. 35, 2000, pp.6251-6258.

[67] R. Hui, W. Cook, C. Sun, Y. Xie, P. Yao, J. Miles, R. Olive, J. Li, W. Zheng and L. Zhang, “Deposition, characterization and performance evaluation of ceramic coatings on metallic substrates for supercritical water-cooled reactors”, Surface and Coatings Technology, Vol. 205, 2011, pp. 3512-3519.

[68] S. Tsipas, J.M. Brossard, M.P. Hierro, J.A. Trilleros, L. Sánchez, F.J. Bolívar and F.J. Pérez, “Al-Mn CVD-FBR protective coatings for hot corrosion application”, Surface and Coatings Technology, Vol. 201, 2007, pp. 4489-4485.

[69] F. J. Perez and S. I. Castaneda, “TG–mass spectrometry studies in coating design for supercritical steam turbines”, Materials and Corrosion, Vol. 59, No. 5, 2008, pp. 409-413.

[70] A. Agüero, R. Muelas, M. Gutiérrez, R. Van Vulpen, S. Osgerby and J.P. Banks, “Cyclic oxidation and mechanical behaviour of slurry aluminide coatings for steam turbine components”, Surface and Coatings Technology, Vol. 201, 2007, pp. 6253-6260.

[71] S. Korablov, B. Basavalingu and M. Yoshimura, “Wet corrosion of nitride PVD films in supercritical solutions”, Corrosion Science, Vol. 47, 2005, pp. 1384-1402.

[72] S. Korablov and M. Yoshimura, “Hydrothermal corrosion of TiN PVD films on SUS-304”, Corrosion Science, Vol. 45, 2003, pp. 531-543.

[73] S. Korablov, M.A.M. Ibrahim and M. Yoshimura, “Hydrothermal corrosion of TiAlN and CrN PVD films on stainless steel”, Corrosion Science, Vol. 47, 2005, pp. 1839-1854.

[74] M. Nagae, Y. Koyama, S. Yasutake and T. Yoshio, “Corrosion behavior of sialon ceramics in supercritical water”, J. Am. Ceram. Soc, Vol. 89, No. 11, 2006, pp. 3550-3553.

[75] E. Barringer, Z. Faiztompkins and H. Feinroth, “Corrosion of CVD Silicon Carbide in 500℃ Supercritical Water”, J. Am. Ceram. Soc, Vol. 90, No. 1, 2007, pp. 315-318.

[76] E. Proverbio and F. Carassiti, “Low-temperature oxidation of silicon nitride by water in supercritical condition”, Journal of the European Ceramic Society, Vol. 16, 1996, pp. 1121-1126.

[77] A.A. Ashary and R.C. Tucker, Jr., “Electrochemical and long-term corrosion studies of several alloys in bare condition and plasma sprayed with Cr_2O_3”, Surface and Coatings Technology, Vol. 43/44, 1990, pp. 567-576.

[78] C.L. Li, H.X. Zhao, M. Matsumura, T. Takahashi, M. Asahara and H. Yamaguchi, “The effect of NiCr intermediate layer on corrosion behavior of Cr_2O_3 ceramic coated materials”, Surface and Coatings Technology, Vol. 124, 2000, pp. 53-60.

[79] L. Zhu, X. Peng, J. Yan and F. Wang, “Oxidation of a novel chromium coating with CeO_2 dispersions”, Oxidation of Metals, Vol. 62, 2004, pp. 411-426.

[80] S. Boudin, J-L. Vignes, G. Lorang, M. Da Cunha Belo, G. Blondiaux, S. M. Mikhailov, J.P. Jacobs and H.H. Brongersma, “Analytical and electrochemical study of passive films formed on nickel-chromium alloys: influence of the chromium bulk concentration”, Surface and Interface Analysis, Vol. 22, 1994, pp. 462-466.

[81] F.H. Stott, “Developments in understanding the mechanisms of growth of protective scales on high-temperature alloys”, Materials Characterization, Vol. 28, 1992, pp. 311-325.

[82] F. Riffard, H. Buscail, E. Caudron, R. Cueff, C. Issartel, S. El Messki and S. Perrrier, “A new interpretation of the ‘breakaway’ oxidation behaviour observed

at high temperature on 304 stainless steel", Materials Science Forum, Vol. 461-464, 2004, pp. 175-182.

[83] A. Ul-Hamid, "TEM study of scale microstructures formed on Ni-10Cr and Ni-10Cr-5Al alloys with and without Y addition", Oxidation of Metals, Vol. 58, No. 1-2, 2002, pp. 41-56.

[84] H-J. Lim, S-W. Park and S-G. Kang, "The effect of particle size of alumina dispersions on the oxidation resistance of Ni-Cr alloys", Oxidation of Metals, Vol. 48, No. 5-6, 1997, pp. 391-415.

[85] F.H. Stott, G.C. Wood and J. Stringer, "The influence of alloying elements on the development and maintenance of protective scales", Oxidation of Metals, Vol. 44, No. 1-2, 1995, pp. 113-145.

[86] F-R. Chen, R. Brown, "Cyclic hot corrosion of Haynes 230 alloy", Journal of Materials Science, Vol. 27, 1992, pp. 2367-2376.

[87] W.G. Cook and R. Olive, "Pourbaix diagrams for iron, nickel, and chromium in sub-critical and supercritical water", The 2nd Canada-China Joint Workshop on Supercritical Water-Cooled Reactors, Toronto, Canada, 2010, April 25-28.

[88] W. Wagner and A. Pruss, "The IAPWS formulation 1995 for the thermodynamic properties of ordinary water substance for general and scientific use", J. Phys. Chem. Ref. Data, Vol. 31, No. 2, 2002, pp. 387-535.

[89] W.H. Bragg and W.L. Bragg, "The reflection of X-rays by crystals", Proc. R. Soc. Lond., Vol. 88, 1913, pp. 428-438.

[90] Z. Dong, W. Chen, W. Zheng and D. Guzonas, “Effect of yttria addition on the stability of porous chromium oxide ceramics in supercritical water”, Journal of Nuclear Materials, 2012, accepted.

[91] P.G. Harrison, N.C. Lloyd, and W. Daniell, “The nature of the chromium species formed during the thermal activation of chromium-promoted tin (IV) oxide catalysts: an EPR and XPS study”, J. Phys. Chem. B, Vol. 102, 1998, pp. 10672-10679.

[92] L. Davydov, E.P. Reddy, P. France, and P.G. Smirniotis, “Transition-metal-substituted titania-loaded MCM-41 as photocatalysts for the degradation of aqueous organics in visible light”, Journal of Catalysis, Vol. 203, 2001, pp. 157-167.

[93] S. Kume, M. Yasuoka, N. Omura and K. Watari, “Effects of MgO addition on the density and dielectric loss of AlN ceramics sintered in presence of Y2O3”, Journal of the European Ceramic Society, Vol. 25, 2005, pp. 2791-2794.

[94] K. L. Gavrilov, S. J. Bennison, K.R. Mikeska and R. Levi-Setti, “Grain boundary chemistry of alumina by high-resolution imaging SIMS”, Acta mater., Vol. 47, No. 15, 1999, pp. 4031-4039.

[95] H. J. Grabke, “Surface and interface segregation in the oxidation of metals”, Surf. Interface Anal., Vol. 30, 2000, pp. 112-119.

[96] S. Chevalie and J.P. Larpin, “Influence of reactive element oxide coatings on the high temperature cyclic oxidation of chromia-forming steels”, Materials Science and Engineering, Vol. A263, 2003, pp. 116-125.

[97] A. Kumar and D.L. Douglass, “Modification of the oxidation behavior of high-purity austenitic Fe-14Cr-14Ni by the addition of silicon”, Oxidation of Metals, Vol. 10, No. 1, 1976, pp. 1-22.

[98] K.R. Mikeska and S.J. Bennison, “Corrosion of alumina in aqueous hydrofluoric acid”, J. Am. Ceram. Soc., Vol. 82, No. 12, 1999, pp. 3561-3566.

[99] A.M. Alper, R.N. Mcnally, R.C. Doman and F.O, Keihn, “Phase equilibria in the system MgO-$MgCr_2O_4$”, J. Am. Ceram. Soc., Vol. 47, No. 1, 1964, pp. 30-33.

[100] E. Nes, N. Ryum and O. Hunderi, “On the Zener drag”, Acta Metallurgica, Vol. 33, No. 1, 1985, pp. 11-22.

[101] N. Moelans, B. Blanpain, P. Wollants, “Pinning effect of second-phase particles on grain growth in polycrystalline films studied by 3-D phase field simulations”, Acta Materialia, Vol. 55, 2007, pp. 2173-2182.

[102] S. Lee, “Dielectric properties of (Ba,Sr,Ca)TiO_3 ceramics modified with MgO for phased array applications”, Journal of the Korean Physical Society, Vol. 41, No. 1, 2002, pp. 129-133.

[103] M. Lei, S. Li, X. Jiao, J. Li and M. A. Alim, “The influence of CeO_2 on the microstructure and electrical behaviour of ZnO-Bi_2O_3 based varistors”, Journal of Physics D: Applied Physics, Vol. 37, 2004, pp. 804-812.

[104] K. Park and S.J. Yun, “Effect of SiO_2 addition on the electrical stability of $(Mn_{2.1-x}Ni_{0.9}Si_x)O_4$ $(0 \le x \le 18)$ negative temperature coefficient thermistors”, Materials Letters, Vol. 58, 2004, pp. 933– 937.

[105] J.S. Park and H.G. Kim, “Electrical conductivity and defect models of MgO-doped Cr_2O_3”, Journal of the American Ceramic Society, Vol. 71, 1988, pp. 173-176.

[106] L. F. Chekhomova, “Abrasive properties of modified chromia”, Inorganic Materials, Vol. 37, No. 3, 2001, pp. 274-280.

[107] M.L. Keith, “Phase equilibria in the system MgO-Cr_2O_3-SiO_2”, Journal of the American Ceramic Society, Vol. 37, No. 10, 1954, pp. 490-496.

[108] D.P. Moon, “The reactive element effect on the growth rate of nickel oxide scales at high temperature”, Oxidation of Metals, Vol. 32, 1989, pp. 47-66.

[109] H.G. Wendlandt and O. Glemser, “The reaction of oxides with water at high pressures and temperatures”, Angew. Chem. intrrnat. Edit, Vol. 3, No. 1, 1964, pp. 47-54.